International Journal of Concrete Structures and Materials

RESEARCH Open Access

Finite-Element Analysis of Flexural Strengthening Performance of Fire-Damaged RC Beams

Lybundith Eng[1] and Changhyuk Kim[1*]

Abstract

In this study, a simplified cross-sectional approach based on finite-element analysis was developed to evaluate the flexural strengthening performance of fire-damaged RC beams using externally bonded steel plates and CFRP strips. The strength degradation of the simplified concrete cross section and reinforcing bars was determined based on the temperature field calculation results from FE software. The strength degradation models proposed in previous literature were adopted and applied based on the obtained temperature distribution. The finite-element model was validated with the previous experimental test to evaluate the accuracy of the model in predicting the residual flexural capacity of RC beams after fire exposure. It is shown that the finite-element model (FEM) was able to predict the flexural behavior of fire-damaged RC members reasonably well. The ISO-834 standard fire curve was applied to the reference flexure beam for 60 min, 90 min, and 120 min of heating before strengthening by employing the proposed methodology. The parametric study in this investigation includes the thickness and width of the strengthening materials for the comparison of the flexural capacity recovery of both retrofitting methods. The analysis results showed that the ultimate load and stiffness of fire-damaged beams strengthened with both materials improved significantly compared to the heated beams without strengthening. The damaged beams group retrofitted with externally bonded steel plates exhibited a greater increase in both ultimate load and stiffness compared to the damaged beams group retrofitted with externally bonded CFRP strips.

Keywords RC beam, Fire damage, Finite-element analysis, Flexural strengthening, Externally bonded reinforcement (EBR), Steel plate, CFRP strips

1 Introduction

Reinforced concrete (RC) exhibits relatively good fire resistance compared to other building materials (Huang, 2010; Thanaraj et al., 2020). The high thermal capacity, low thermal conductivity, and slow degradation of the mechanical properties of concrete during fire can protect the reinforcing bars from excessively high-temperature exposure. Therefore, in most cases, RC members can be reused after a fire event (Ma et al., 2019). Although RC members can still be reused, the original design criteria of the structure may not be satisfied. Thus, strengthening is required to restore the designed ultimate structural capacity of fire-damaged RC members. Various strengthening techniques for existing RC structures have been applied, including section enlargement (Hao et al., 2022; Wang et al., 2013; Yang, 2019), externally bonded steel plate (Alam et al., 2020; Altin et al., 2005; Baluch et al., 1995; Ciampa et al., 2023; Hamoda et al., 2023; Hamoush & Ahmad, 1990), external prestressing (Lou et al., 2012, 2013; Tianlai et al., 2016), replacement of damaged concrete, externally bonding or near-surface mounting of carbon FRP (Abdallah et al., 2020; Haroon et al., 2021; Kim et al., 2017), glass FRP

*Correspondence:
Changhyuk Kim
changhyuk@inha.ac.kr
[1] Department of Architectural Engineering, Inha University, Incheon 22212, Republic of Korea

(Sundarraja & Rajamohan, 2009), and basalt FRP (Kar & Biswal, 2021) composite materials.

Many experimental studies regarding the strengthening of fire-damaged RC members have increased in the last decade. Shang et al. (2020) used stirrup-reinforced engineered cementitious composites (ECC) to strengthen fire-damaged RC beams in shear after exposure to the ISO 834 heating curve for 2 h. Another experimental test was carried out by da Costa et al. (2023). Thirteen RC beams were exposed to the ISO 834 heating curve for durations of 60, 90, and 120 min. Near-surface-mounted CFRP laminates were applied at spacings of 75, 150, and 200 mm for shear strengthening. Anasco Bastin et al. (2017) experimentally investigated the strengthening effect of high-strength fiber-reinforced concrete (HSFRC), ferrocement (FC) jacketing, and externally bonded fiber-reinforced polymer (FRP) on fire-damaged T-beam. This study concluded that externally bonded FRP was determined to be the most effective strengthening method among all. Mejía et al. (2024) conducted experimental tests to evaluate the shear and flexural strengthening performance of post-fire damaged RC beams using externally bonded CFRP sheets. An experimental study conducted by Li et al. (2022) was to study the flexural performance of eight full-scale beams damaged by fire. Strain-hardening cementitious composite (SHCC) and basalt-fiber-reinforced polymer fabric were used as strengthening matertials. Jiang et al. (2017), Li et al. (2019) experimentally studied the shear and flexural performance of fire-damaged RC beams using the bolted side-plating (BSP) technique. Aldhafairi et al. (2020) conducted experimental and analytical research on the effectiveness of steel jacketing in normal-strength concrete, high-strength concrete, and self-compacting concrete beams after exposure to elevated temperatures. The experimental studies reviewed have employed various strengthening materials and techniques for both shear and flexural strengthening of fire-damaged beams. Compared to other strengthening materials investigated, steel plate strengthening using the externally bonded reinforcement (EBR) method has received less attention in the application of flexural strengthening for fire-damaged beams. Externally bonded steel plating has been widely used for strengthening of RC members over the last few decades (Barnes & Mays, 2006; Thamrin & Sari, 2017; Vilnay, 1988; Zhang et al., 2001) due to its ease of application, low material costs, minimal disruption to the structure, and less skilled labor requirements compared to other strengthening materials and techniques (Aykac et al., 2013). Therefore, externally bonded steel plates should also be given consideration in the repair applications of fire-damaged beams. The application of strengthening using externally bonded CFRP on fire-damaged beams has been observed to be limited. The application of externally bonded CFRP has been experimentally investigated by Anasco Bastin et al. (2017) and Mejía et al. (2024). However, these studies did not consider the variation in strengthening effects due to different widths and thicknesses of CFRP application. The use of CFRP material as externally bonded on existing RC members has been increased. This is due to the high tensile strength, excellent corrosion resistance, high strength-to-weight ratio, ease of installation, and low thermal conductivity of the materials (Fayyadh & Razak, 2021; Moon et al., 2023; Oller et al., 2019). The use of externally bonded CFRP should be considered for the repair of fire-damaged beams, with the strengthening effects of CFRP thickness and width also taken into account.

Numerical models based on the finite-element method (FEM) have been developed to study the effect of fire and the strengthening performance of RC members exposed to high temperatures due to the time and cost consumption of fire testing and certain phenomena that are exceedingly challenging to observe experimentally. Jadooe et al., (2017) numerically simulated the behaviour of heat-damaged RC beams strengthened with NSM CFRP laminate using epoxy and cement-based adhesive. The proposed finite-element models (FEMs) accurately predicted experimental behavior. Later, Jadooe et al., (2018a), Jadooe et al., (2018b), developed another finite-element model to examine the behavior of NSM CFRP-strengthened heated beams, considering concrete top surface insulation with cement-based adhesive and epoxy-based adhesive, respectively. However, the heating curves considered in their study were limited to a maximum temperature of 800 °C. Sabar and Kadhum, (2022) investigated the behavior of fire-damaged high-strength lightweight RC beams strengthened with a SIFCON jacket using the finite-element method by the ABAQUS program. The highest heating temperature in the study by Sabar and Kadhum, (2022) was limited to 600 °C, with a heating duration of 60 min.

Belakhdar et al., (2023) conducted a numerical investigation on the strengthening performance of steel jacketing after exposure to fire for different durations of 15, 30, 60, and 90 min. This study examined the effect of various steel jacket configurations on the concrete, including steel corner jackets, vertical steel jackets, and horizontal jackets. Different heating durations and steel plate jacketing schemes were examined. However, the variation in the thickness and width of the plates was not considered in their study. In a recent study, Shareef and Kadhum, (2025) proposed a numerical model to examine the effect

of a new composite strengthening method using a basalt fiber-reinforced polymer (BFRP) grid combined with an engineered cementitious composites (ECC) matrix to repair the strength of fire-damaged lightweight high-strength concrete beams for 60 min. The new composite strengthening method was investigated in the study; however, the heating duration was limited to 60 min. The previously proposed numerical methods by researchers utilized detailed finite-element analysis to investigate the effects of strengthening fire-damaged beams. These methods demonstrated high accuracy in evaluating the residual capacity and strengthening performance of fire-damaged RC members. However, this method simulated the heating phase, cooling phase, implementation of the strengthening scheme and materials, and applied loading within a single analytical framework. The application of thermal load was significant and required multiple steps, which could potentially lead to convergence issues during the analysis. Moreover, certain repair techniques widely applied to fire-damaged members, such as the concrete enlargement technique, damaged concrete replacement technique, and outer concrete removal prior to strengthening, were found to be challenging to simulate using detailed finite-element methods. This is because such repair techniques involve adding new concrete and replacing damaged old concrete, which is difficult to simulate and analyze within a single analytical framework.

Therefore, this research study aims to propose a simplified analytical approach to evaluate the flexural strengthening effect using externally bonded steel plate and CFRP strips. In the simplified approach, the cross section of the fire-damaged beam was divided into different segments based on the maximum temperature at the end of the heating regimes. The strength degradation of each concrete segment and reinforcement bar was modified according to the temperatures obtained from the FE software. Based on the simplified cross-sectional approach, the residual capacity of fire-damaged RC beams was first analyzed, and the accuracy of the numerical model was verified with reference experimental tests. Using the numerical model, one reference RC beam was subjected to the ISO standard heating curve for durations of 60, 90, and 120 min. Fire-damaged beams were then strengthened in flexure with different widths and thicknesses for evaluating the flexural performance.

2 Analytical Methodology

2.1 Thermal Analysis in ATENA–GiD

ATENA–GiD has been widely utilized in many analytical research studies for the thermal analysis of RC members (Cervenka et al., 2020; Jadooe et al., 2017, 2018a, 2018b; Sadaghian et al., 2023). Among those researches, Jadooe et al. (2018a) compared the FEM and experimental time–temperature curves of the concrete beam surface, 46 mm from the core of the concrete beam, core of the concrete beam, and the middle of the reinforcing bar under heating regimes of 700 °C and 800 °C. The four thermocouples reading temperature in the heating test showed good correspondence with the FEM calculated temperatures. The research concluded that finite-element analysis using ATENA–GiD calculated the heat transport in RC beams reasonably well. Similar conclusions were also drawn by other research studies (Jadooe et al., 2017, 2018b). It can be concluded that heat transport analysis carried out with ATENA–GiD is reliable for heat transfer and thermal analysis of RC members.

In this study, the heat transport model of RC members was constructed in ATENA–GiD considering the concrete material properties and the surface temperature conditions of the heating surfaces of the RC members. The heat transport analysis was performed on the assumption that the RC members consisted entirely of concrete material. The concrete material model enables users to input different parameters, such as thermal conductivity, heat capacity, and the initial temperature of the concrete for fire exposure.

The heat transport by ATENA used Fourier law to predict the evolution of temperature fields in the structure (Jendele et al., 2014):

$$\frac{\partial}{\partial t}(Q) = -div\left(\overline{q}_T\right) \tag{1}$$

where Q represents the total heat accumulated per unit volume of concrete and $\overline{q}_T$ is the heat flux:

$$\frac{\partial Q}{\partial t} = \frac{\partial Q_c}{\partial T}\frac{\partial T}{\partial t} + \frac{Q_h}{\partial t} = C_T\frac{\partial T}{\partial t} + \frac{\partial Q_h}{\partial t} \tag{2}$$

where Q_c represents the heat gain or loss due to conduction, C_T is the heat capacity, and Q_h is the total hydration heat released at time (t):

$$\overline{q}_T = -\lambda\nabla(T) \tag{3}$$

where λ is thermal conductivity. The unknown temperature can be calculated by substituting Eqs. (2) and (3) in Eq. (1).

To make the surface time–temperature history variation of FEM align with the experiment heating tests, Dirichlet temperature conditions for the surface were used. With the help of interval data settings, the heating temperatures as a function of time from the experimental test can be applied to the surfaces of RC members. The results of the heat transport analysis were then imported into the static analysis model to calculate the temperature of the reinforcement bars. ATENA–GiD static analysis

permits the calculated temperature from heat transport analysis results to be correlated with reinforcing elements depending on the location of reinforcement bars within concrete. Therefore, rebar's temperature changes throughout the analysis can be measured using monitoring for line elements in static analysis.

2.2 Static Analysis in ATENA 3D

Nonlinear finite-element analysis of the post-fire residual capacity and flexural strengthening performance of fire-damaged RC members under static load was conducted using ATENA 3D software. Finite-element models using ATENA 3D were developed by many researchers to examine the behavior of RC members and the efficacy of various strengthening materials. Joyklad et al., (2023) carried out an experimental test on the structural behavior of a full-scale precast post-tensioned girder with substandard transverse reinforcement. Finite-element analysis by ATENA 3D was developed to compare with experimental results. Good accuracy was reported on load–deflection response and cracking patterns between experimental and analysis results. Analytical research conducted by Moon et al., (2023) indicated that the FE model using ATENA 3D accurately described the behavior of CFRP-strengthened RC beams.

In this study, the residual flexural capacity of RC members after fire was assessed by dividing the cross section to analyze concrete strength deterioration based on temperature distribution at the end of the heating regime obtained from thermal analysis results. The deterioration in elastic modulus and yield strength of reinforcing bars due to increased temperature, as measured via thermal analysis, were calculated following a simplified stress–strain model after elevated temperature developed by Tao et al., (2013). The strength of reinforcing bars exhibits notable recovery upon cooling down to ambient temperature (Büyüköztürk et al., 2013), and the residual strength of rebars has a significant influence on the flexural capacity of RC members after fire (Kodur & Agrawal, 2016). Therefore, the strength degradation model of rebar after fire proposed by Tao et al., (2013) was considered for this analytical investigation. In the case of concrete, unlike rebar, which exhibits significant strength recovery upon cooling, concrete does not demonstrate any significant regain in strength after being cooled down to ambient temperature. Therefore, Eurocode (2004) was used for the calculation of the elastic modulus and compressive strength degradation of concrete subjected to elevated temperatures.

Concrete was modeled as a fracture–plastic constitutive model for brittle materials. Figure 1a shows the fracture concept of the concrete, which is based on the uniaxial stress–strain response. Both linearity in tension and compression are considered in this ATENA built-in material model. The behavior of concrete without cracks in tension was assumed to be linear elastic. In the case of the post-cracking tensile behavior of concrete, a fictitious crack model based on crack-opening law and fracture energy was used. This formulation is suitable for the modeling of crack propagation in concrete (Červenka et al., 2021). 1D truss element (*reinforcement*) was used for the modeling of reinforcing bars. Rebars were assumed to be elastic-perfectly plastic, and the bilinear constitutive model shown in Fig. 1b was used. Bond behavior between concrete and rebar differs at ambient temperatures, elevated temperatures, and after fire exposure, requiring a different bond slip model for each condition. However, for simplification, this research assumed perfect bond behavior between rebars and concrete. For the modeling of strengthening CFRP sheets, the material model was adopted using the modeling approach by Moon et al., (2023). This modeling approach simplifies CFRP material by creating a three-dimensional element that represents a saturant-base material with a thickness equal to a CFRP sheet. The saturant material (epoxy) was assigned with the isotropic linear elastic material model with reinforcement. Bilinear with hardening reinforcement was used to determine the rupture strain of CFRP. The fibers were defined as smeared reinforcement with a reinforcement ratio of 100%. The stress–strain relationship of CFRP is shown in Fig. 1c. Strengthening steel plates were simulated using the bilinear steel Von Mises model in ATENA presented in Fig. 1b. Su et al., (2008) also implemented the bilinear steel Von Mises model for simulating steel plates in their study. This model used the biaxial failure law combined with the bi-linear stress–strain law to account for the elastic state and hardening of steel (Su et al., 2008). Using a similar modeling approach as CFRP, a new 3D element was constructed with the same thickness as the steel plate. A bilinear steel Von Mises model was then assigned to the newly created 3D element.

3 Verification of Finite-Element Model

3.1 Experiemental Tests by Jadooe et al. (2017)

The residual flexural capacity of the concrete beam after elevated temperature tested by Jadooe et al., (2017) was analyzed by employing the above modeling procedure to validate the numerical model. The loading points and reinforcement details of the tested RC beam are shown in Fig. 2. The dimensions of the investigated beam were 140 mm in width, 260 mm in depth, and 2700 mm in length. Three bars of D12 were used for tensile reinforcement, while two bars of D12 were used as compressive rebars. D10 was used as shear reinforcement with spacings of 120 mm. The specimens were tested at the age

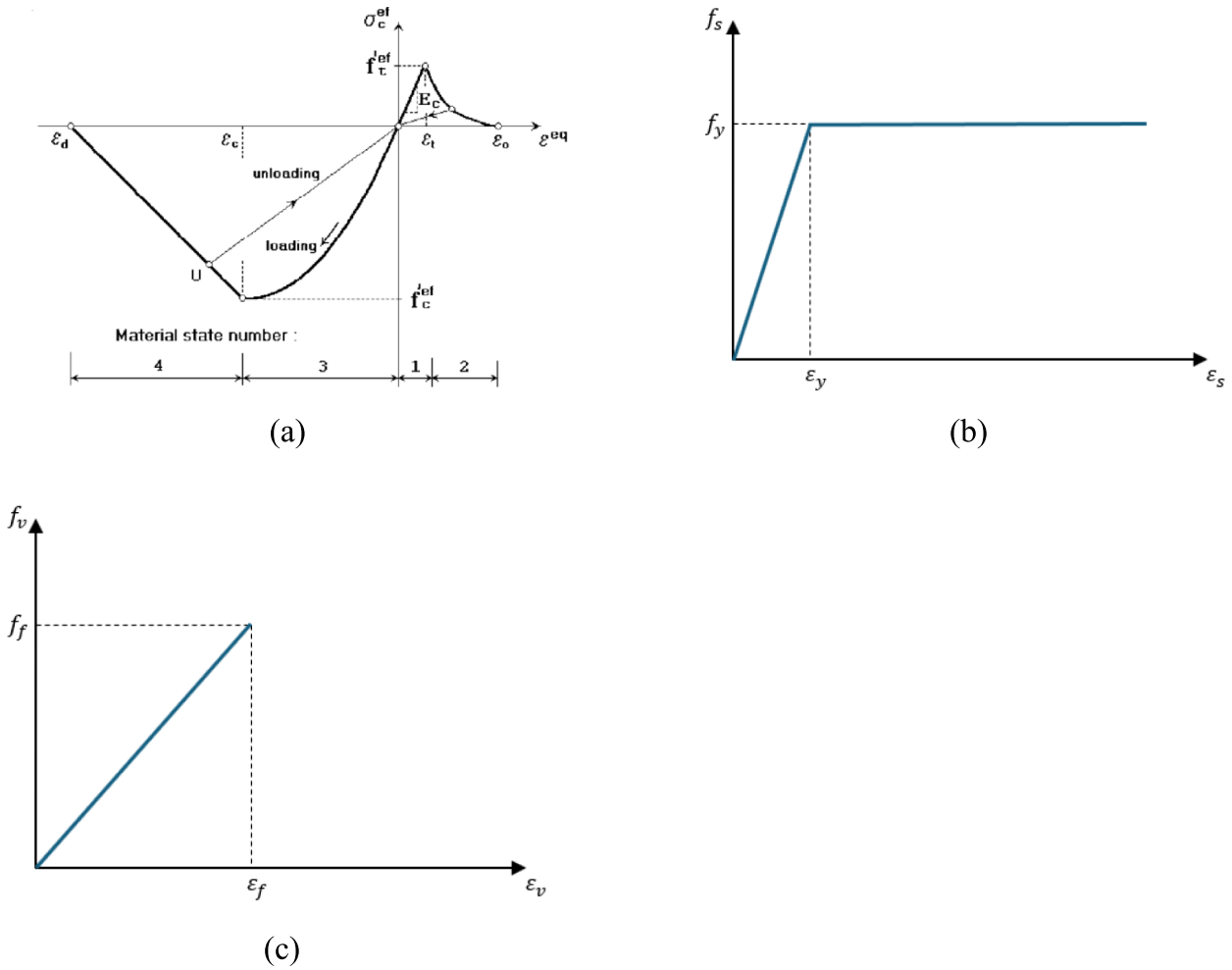

Fig. 1 Constitutive materials models. **a** Uniaxial stress–strain law of concrete (Červenka et al., 2021), **b** stress–strain relationship of rebar and steel plate, **c** stress–strain relationship of CFRP

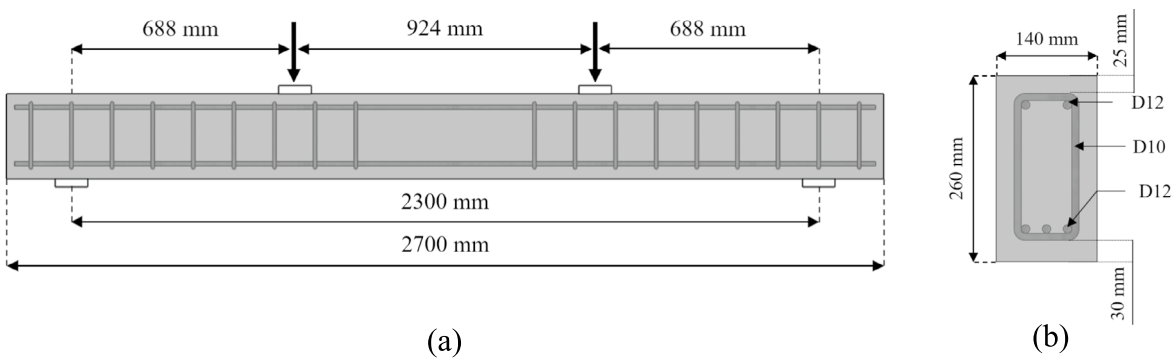

Fig. 2 Details of the beam specimens. **a** Loading arrangement. **b** Section details

of 10 months after casting and the average compressive strength of the concrete was 38.6 MPa. D12 rebars had an average yield strength and elastic modulus of 587 MPa and 209 GPa, while the material properties of D10 rebars were 561 MPa and 206 GPa, respectively. The RC beam was heated on four surfaces to reach a maximum

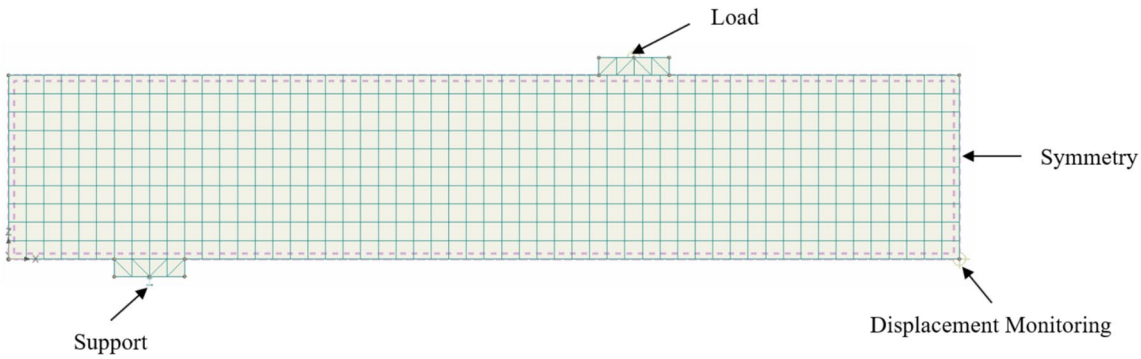

Fig. 3 Unheated RC beam model

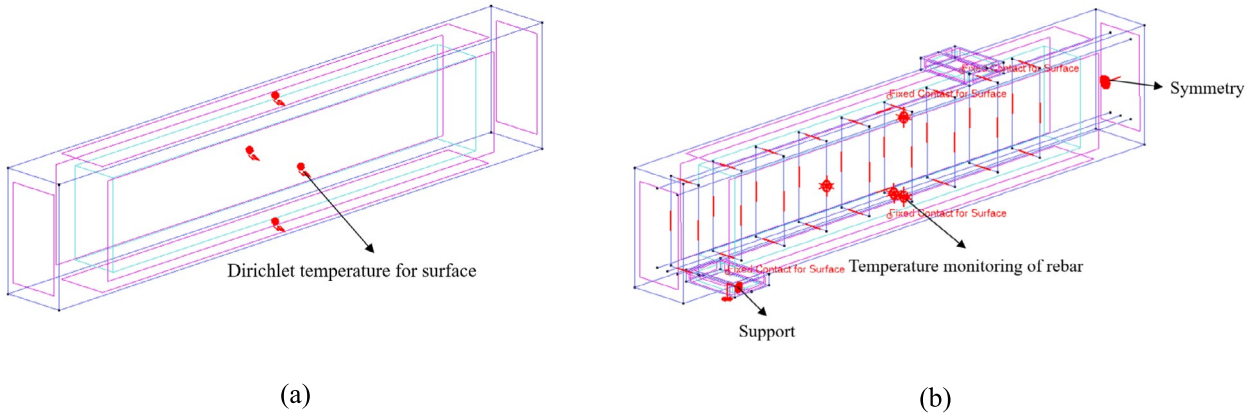

Fig. 4 ATENA–GiD RC beam models. **a** Heat transport model. **b** Static model

temperature of 600 °C and kept heated at the target temperature constant for 2 h before cooling down to ambient temperature.

3.1.1 Finite-Element Analysis of Heated RC Beam

The unheated RC beam was constructed using ATENA 3D software to verify with the unheated control beam in the experimental test, as shown in Fig. 3. The material properties of concrete and reinforcing bars were determined by the material properties tested in the experiment. Due to symmetry, only half of the RC beam was modeled to reduce the computation time.

ATENA–GiD was employed to develop the heat transport model of the RC beam without reinforcement, as presented in Fig. 4a. A separate static model with reinforcement was created to measure the temperature of the rebars throughout the analysis, as shown in Fig. 4b. Two models were developed, as the heat transport model was limited to calculating the temperature field distribution within the concrete. Therefore, a static model was required to determine the temperature of the rebars. The material properties of the concrete model are shown in Table 1. The Dirichlet temperature condition for surfaces was applied to all four surfaces of the RC beam for 2 h. To make the time–temperature heating curve in FEM aligned with the experimental heating test, seven interval data were considered with different temperature increments, as summarized in Table 2. Figure 5 compares the FEM and experimental heating curves of the RC beam. Figure 6 presents the temperature distribution of concrete and rebars after the thermal analysis process.

Table 1 Materials properties for concrete

Thermal conductivity [W/°C.m]	Thermal capacitance [kN/m^2.°C]	Initial temperature [°C]
1.1	2550	25

The static model for the heated RC beam in ATENA 3D was constructed with the same boundary conditions as the unheated beam model. Figure 7a presents the actual temperature distribution of the concrete beam obtained from the thermal analysis results. The simplified

Table 2 Surface temperature regime for FEA

Interval	Number of steps	Starting time (min)	Ending time (min)	Temperature at the start of interval (°C)	Temperature at the end of interval (°C)	Temperature increment(°C)
1	10	0	1	25	350	325
2	10	1	2	350	445	95
3	10	2	3	445	502	57
4	10	3	4	502	545	43
5	10	4	5	545	575	30
6	10	5	6	575	599	24
7	10	6	120	599	600	1

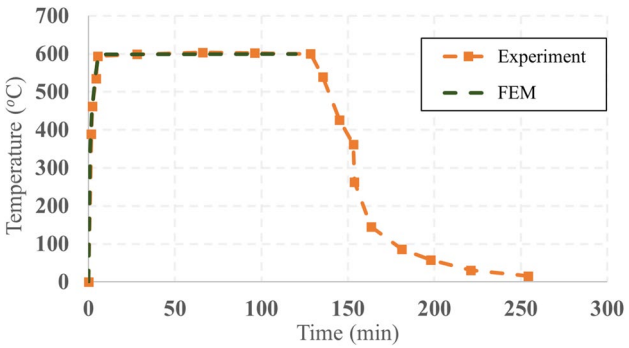

Fig. 5 Comparison of experimental and FEM heating curves

temperature distribution for each concrete cross section of the fire-damaged beam is shown in Fig. 7b. The simplified temperature distributions of the first, second, and third cross sections were 581 °C, 529 °C, and 494 °C, respectively. Figure 7c shows the dimensions of each divided cross section and FE meshes in finite-element software. For the modeling of concrete beams, brick meshes with the size of 0.02 m were used. The strength degradation for each concrete cross section was calculated based on the simplified temperature shown in Fig. 7b. The strength degradation of each reinforcing bar was determined according to the temperatures from the thermal analysis results, as shown in Fig. 6b. Concrete cross section and rebar strength deterioration are shown in Tables 3 and 4, respectively. The interface between concrete cross sections of the RC beam was modeled to be perfectly connected.

3.2 Experiemental Tests by Van Cao et al., (2022)

To increase the reliability of the proposed FE model in evaluating the residual flexural capacity of fire-damaged RC members, an experimental test by Van Cao et al., (2022) was analyzed. The investigated RC slab was simply supported with dimensions of 2000 × 750 × 100 mm. D10 rebars were used with a clear cover of 15 mm. The average compressive strength of concrete at 28 days was 26.02 MPa, and the average yield strength of reinforcing bars was 335.8 MPa. Figure 8 shows the geometry,

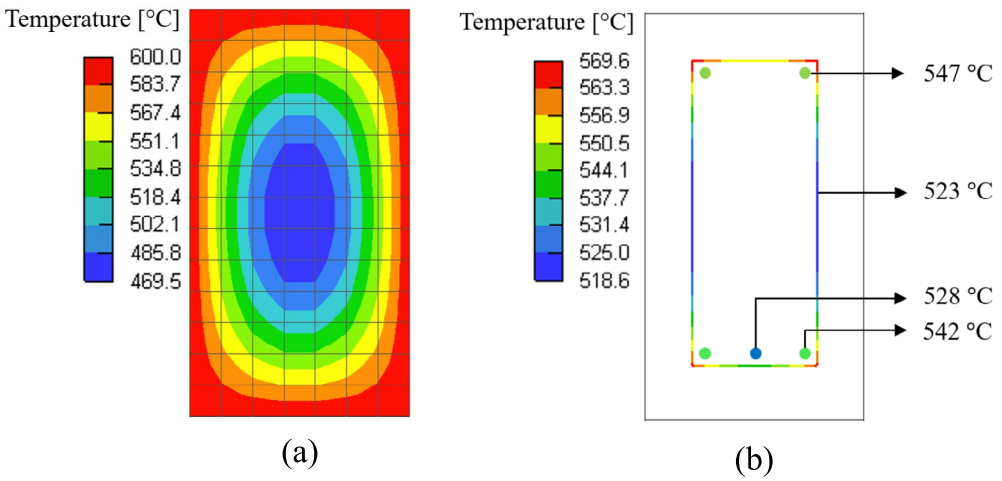

Fig. 6 Temperature distribution of the heated beam. **a** Concrete. **b** Reinforcing bars

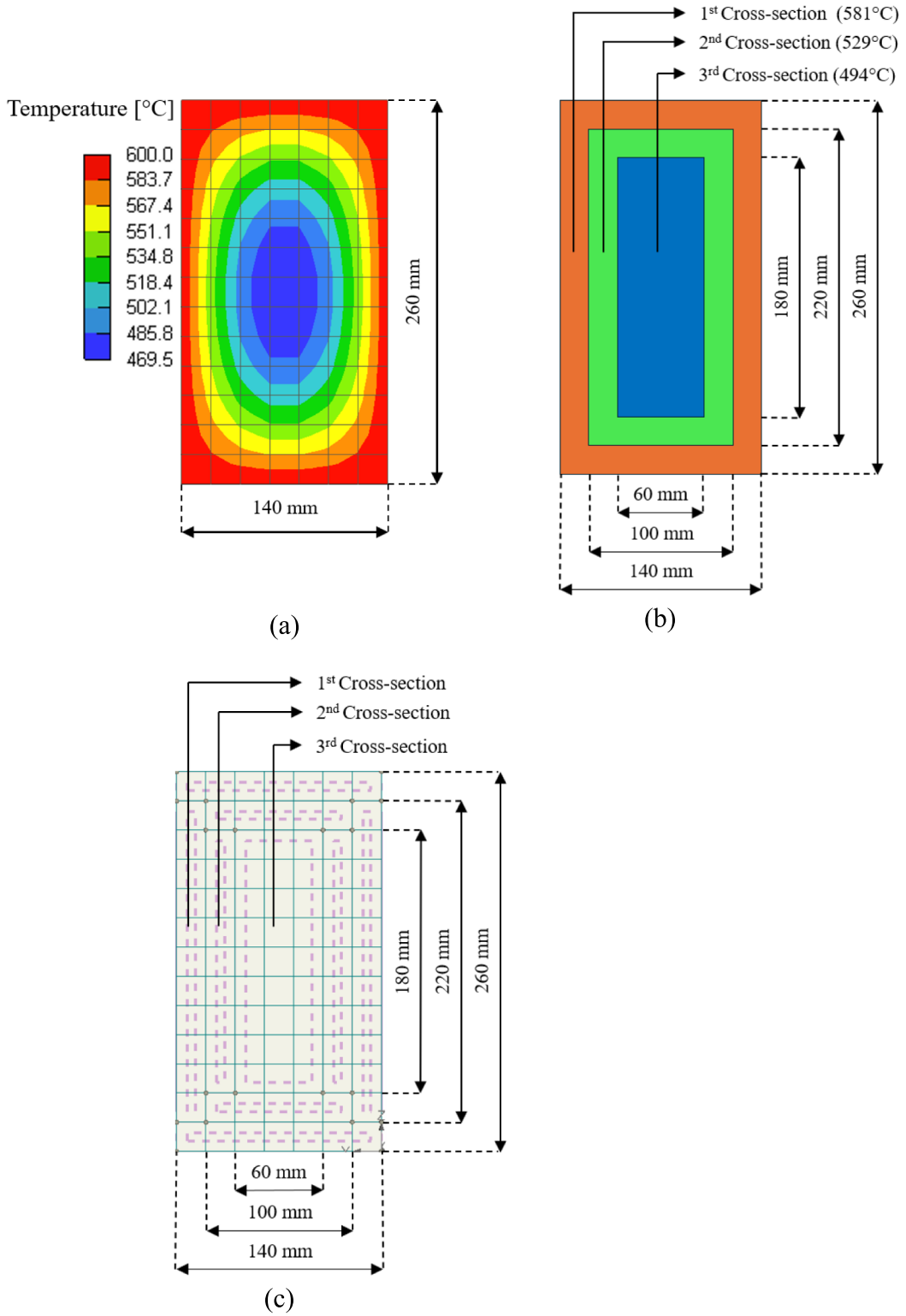

Fig. 7 Temperature and cross section of the concrete beam. **a** Actual temperature distribution. **b** Simplified temperature distribution. **c** Cross-sectional division of the heated beam (FE model)

Table 3 Strength degradation of concrete cross sections

Cross section	1st cross section	2nd cross section	3rd cross section
Temperature (℃)	581	529	494
Compressive Strength (MPa)	18.5	21.5	23.9
Elastic Modulus (MPa)	20,427	22,143	23,529

Table 4 Strength degradation of reinforcing bars

Reinforcing bar	Tensile Rebar (side)	Tensile Rebar (mid)	Compressive Rebar	Stirrup
Temperature (℃)	542	528	547	523
Yield Strength (MPa)	572.7	577.4	571	553.5
Elastic Modulus (MPa)	207,859	208,239	207,723	205,384

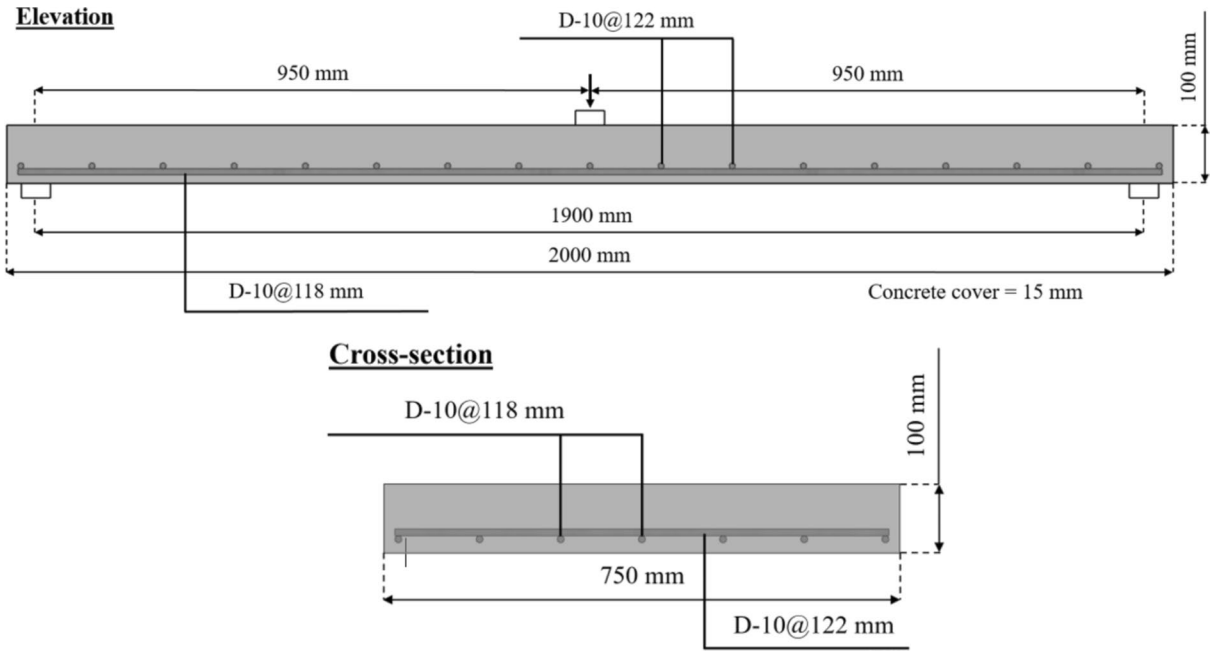

Fig. 8 Geometry, loading, and reinforcement details of the concrete slab

loading, and reinforcement details of the concrete slab model. The RC slabs were heated on the bottom side for 45 min and 75 min, respectively, before the static loading test.

3.2.1 Finite-Element Analysis of Fire-Damaged RC Slab

The same modeling procedure as the heated RC beam was performed. RC slab model was created with temperature increments applied to the bottom surface at intervals of 45 min and 75 min of heating, respectively. To make the bottom surface temperature increment of FEA correspond with the experimental heating curve, eight intervals were divided into different surface temperature increments for 45 min and 75 min of heating. Table 5a, b summarizes the eight intervals of surface temperature increment for 45 min and 75 min of heating, respectively. The comparison of the heating curve between FEM and the experiment of the RC slab for each heating duration is illustrated in Fig. 9a, b. Figure 10 presents the actual temperature distribution of the concrete slab and reinforcing bars based on the thermal analysis results. Figure 11a, b shows the simplified temperature distribution of concrete and the dimensions of the divided cross sections for 45 min and 75 min of heating. Four cross sections were

Table 5 (a) Surface temperature regime for FEA (45 min heating) (b) Surface temperature regime for FEA (75 min heating)

Interval	Number of steps	Starting time (min)	Ending time (min)	Temperature at the start of interval (°C)	Temperature at the end of interval (°C)	Temperature increment(°C)
1	10	0	1.5	25	401	376
2	10	1.5	2	401	568	167
3	10	2	5	568	684	116
4	10	5	11	684	762	78
5	10	11	23	762	838	76
6	10	23	33	838	890	52
7	10	33	40	890	944	54
8	10	40	45	944	964	20
Interval	**Number of steps**	**Starting time (min)**	**Ending time (min)**	**Temperature at the start of interval (°C)**	**Temperature at the end of interval (°C)**	**Temperature increment(°C)**
1	10	0	2	25	427	402
2	10	2	3	427	617	190
3	10	3	5	617	677	60
4	10	5	15	677	738	61
5	10	15	34	738	810	72
6	10	34	51	810	887	77
7	10	51	62	887	949	62
8	10	62	75	949	984	35

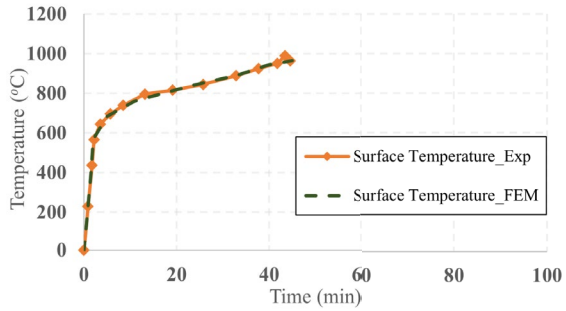

Fig. 9 Comparison of experimental and FEM heating curves. **a** 45 min of heating. **b** 75 min of heating

divided with a thickness of 25 mm for each heated slab. Figure 11c presents the cross-sectional division of the RC slab in FE software. For each concrete slab model, brick meshes with the size of 0.02 m were used. The strength degradation for each concrete cross section was calculated based on the simplified temperature shown in Fig. 11a, b. Tables 6 and 7 summarize the strength degradation of each concrete slab cross section and reinforcing bars for 45 min and 75 min of heating, respectively.

3.3 Comparison of Load–Deflection Responses

The load–deflection response of the RC members was considered the key criterion for evaluating the proposed methodology in comparison with the experimental test. Table 8 presents a comparison of the difference in the percentage of ultimate load and maximum deflection of fire-damaged RC members between FEA and experimental results. The FEA predicted ultimate load and maximum deflection of fire-damaged RC members were less than 10% compared to the experimental results. The exception was the 75-min heated slab, which showed a difference higher than 10% from the test results. Figures 12 and 13 show the comparison of the load–deflection curves of the finite-element analysis results with the experimental results of the heated RC beam and slab, respectively. It can be seen that this finite-element analysis approach was able to reasonably evaluate the residual ultimate load-carrying capacity and deflection of both fire-damaged

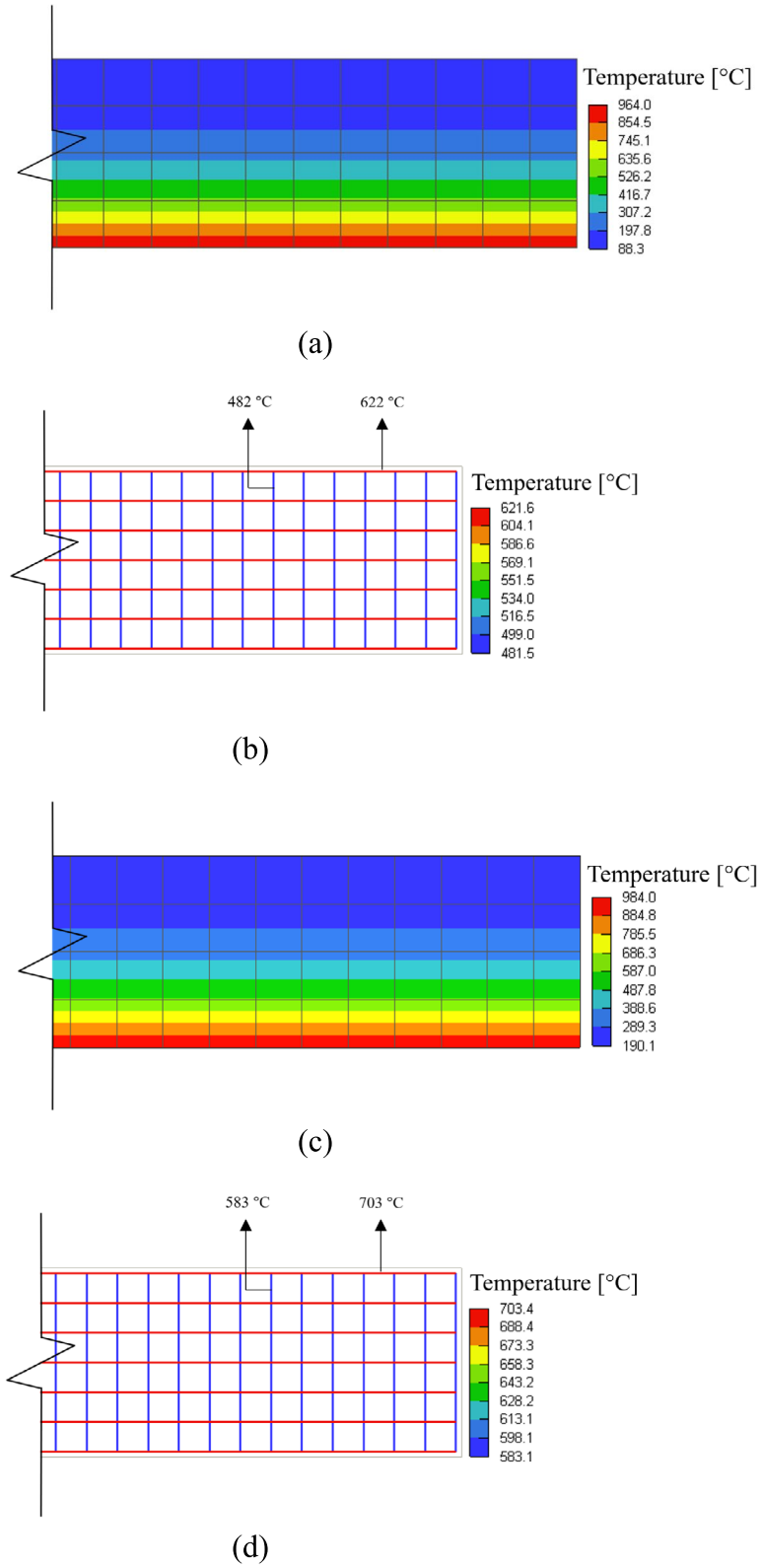

Fig. 10 Temperature distribution of heated RC slab. **a** Concrete (45 min heating). **b** Reinforcing bars (45 min heating). **c** Concrete (75 min heating). **d** Reinforcing bars (75 min heating)

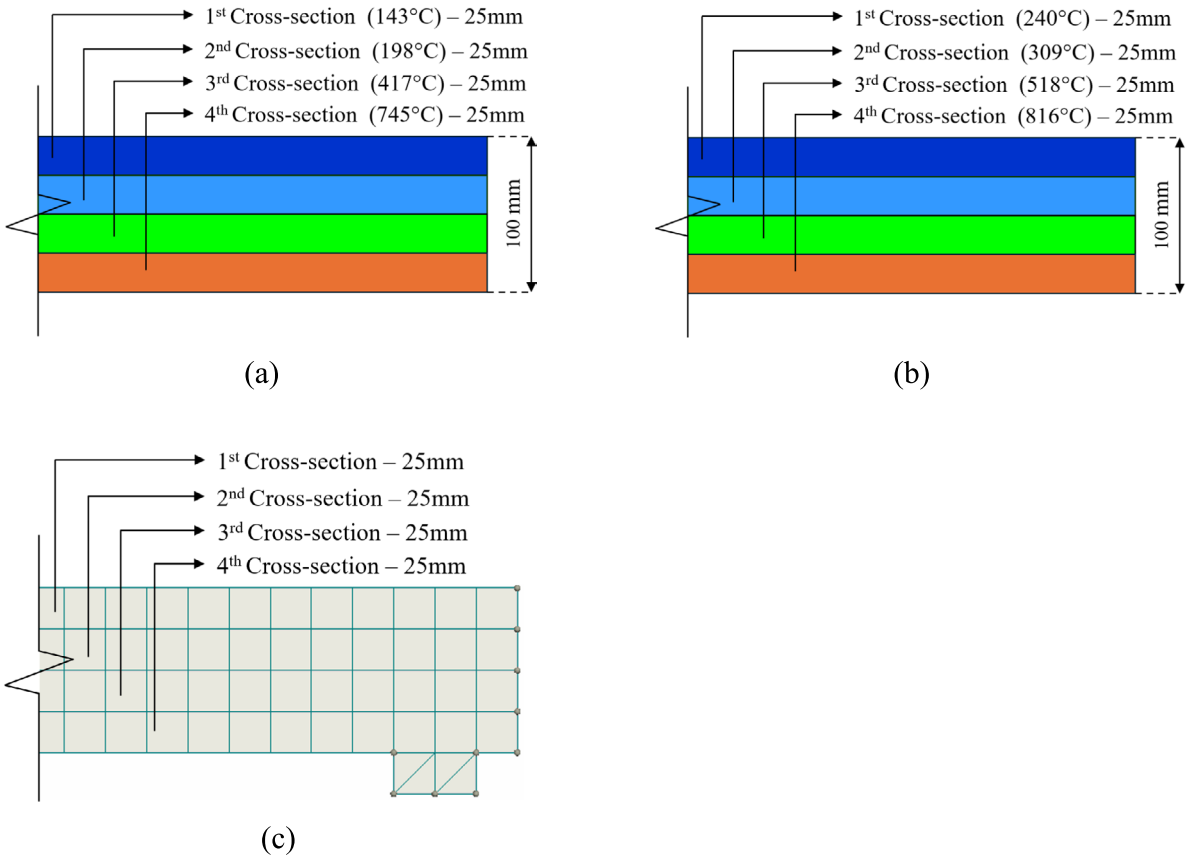

Fig. 11 Simplified temperature and cross section of concrete beam. **a** Simplified concrete temperature distribution (45 min heating). **b** Simplified concrete temperature distribution (75 min heating). **c** Cross-sectional division of heated RC slab (FE model)

Table 6 (a) Strength degradation of concrete cross sections (45 min heating) (b) Strength degradation of concrete cross sections (75 min heating)

Cross section	1st cross section	2nd cross section	3rd cross section	4th cross section
Temperature (℃)	745	417	198	143
Compressive Strength (MPa)	6.1	18.9	24.2	24.2
Elastic Modulus (MPa)	12,990	22,355	28,550	28,550
Temperature (℃)	816	518	309	240
Compressive Strength (MPa)	3.6	14.9	21.9	22.9
Elastic Modulus (MPa)	10,963	19,471	25,438	27,408

RC beams and slabs. However, the analytical stiffness before yielding of fire-damaged members was found to be higher than the experimental results. The main reason for this phenomenon could be the assumption of the perfect connection between concrete and reinforcing bars under both unheated and heated conditions. The observed higher stiffness in the analysis could also be attributed to errors in the installation experimental testing procedures of the RC members (Hussain et al., 2022).

Table 7 (a) Strength degradation of reinforcing bars (45 min heating) (b) Strength degradation of reinforcing bars (75 min heating)

Reinforcing bar	Main bar (D10)	Distribution bar (D10)
Temperature (℃)	622	482
Yield Strength (MPa)	312	335.8
Elastic Modulus (MPa)	205,685	209,000
Temperature (℃)	703	583
Yield Strength (MPa)	296.1	319.6
Elastic Modulus (MPa)	203,484	206,745

4 Strengthening of Fire-Damaged RC Beam

4.1 Exposure to ISO Standard Fire Curve

Reference RC beam specimen from the experiment test by Ahmad and Bhargava, (2023) was chosen for this investigation. The investigated RC beam had a cross-sectional dimension of 230 mm × 400 mm with a length of 4000 mm. The average compressive strength of concrete was 40.3 MPa. 2-D20 and 1-D16 were used for tensile reinforcement, while 2-D8 were used as compressive rebars. D8 stirrup was used for shear reinforcement at a spacing of 170 mm. Table 9 summarizes the material properties of the concrete and reinforcing bars used in the experimental test. The loading arrangement and section details of the tested RC beam specimen are shown in Fig. 14. During the heating phase, only the thermal load was applied, with no additional mechanical loading. Following the heating phase, the beam was subjected to loading to evaluate its residual capacity.

To study the fire effect on the load–deflection response of the RC beam, the reference beam was subjected to ISO standard fire curve for 60 min, 90 min, and 120 min by employing the above modeling approach. The fire exposure surfaces were the bottom and both sides of the beam, simulating actual fire conditions on the beam, where the top surface of the beam is not exposed to fire. Figure 15a, b presents the cross section of the undamaged beam and the fire-damaged beam, respectively. The dimensions of the divided cross sections of the fire-exposed RC beam are shown in Fig. 15b. Tables 10 and 11 summarize the temperature and strength degradation of each concrete cross section and rebar for all heating durations, respectively, according to thermal analysis results.

The predicted load–deflection response of the control unheated beam from the FE model exhibited good agreement with the experimental results, as shown in Fig. 16a. The ultimate load of the experimental result was 261 kN, while the FEA result was 256 kN, which showed only a 2% difference between both results. Figure 16b

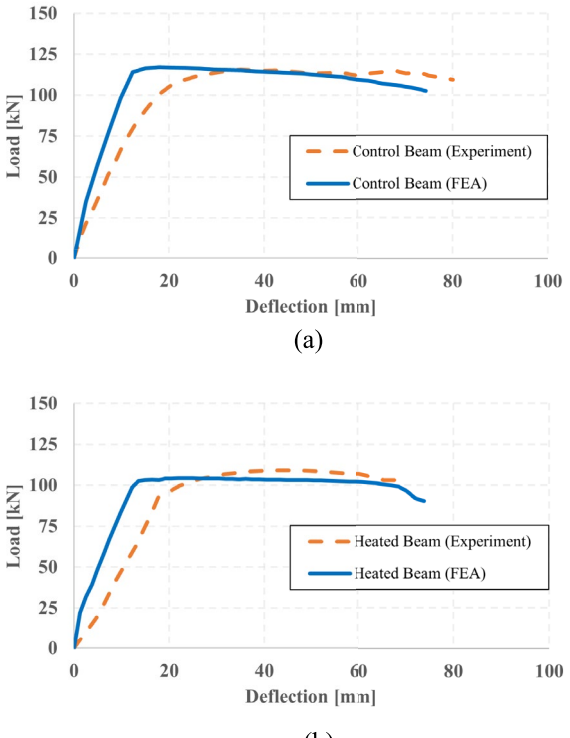

Fig. 12 Comparison of load–deflection curves between experiment and FEA. **a** Control beam. **b** Heated beam

Table 8 Comparison of FEA and experimental results

Specimen	Ultimate Load			Maximum Deflection		
	FEA (kN)	Experiment (kN)	Difference (%)	FEA (mm)	Experiment (mm)	Difference (%)
Control Beam	117.2	115.5	1.5	74.4	80	7.0
Heated Beam	104.3	108.9	4.2	73.9	70.4	5.0
Control Slab	34.1	34.7	1.7	60.3	57.7	4.5
Heated Slab (45 min heating)	32.1	32.7	1.8	60.5	62.9	3.8
Heated Slab (75 min heating)	30	33.5	10.4	60.5	69.7	13.2

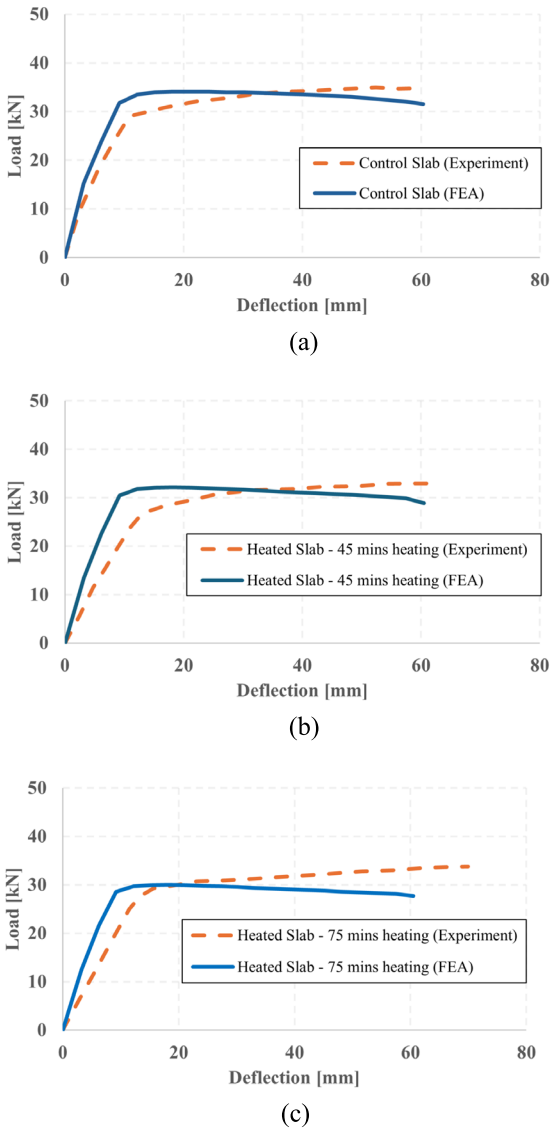

Fig. 13 Comparison of load–deflection curves between experiment and FEA. **a** Control slab. **b** Heated slab (45 min heating). **c** Heated slab (75 min heating)

illustrates the load–deflection response of beams heated for 60 min, 90 min, and 120 min compared to the control beam. In the case of 60 min of heating, the ultimate load was 242 kN, which decreased by about 5.8% compared to the control unheated beam. This small difference in the maximum load of the 60-min heating beam specimen occurred due to the temperature of the tensile rebars, which were only 525 °C and 417 °C after 60 min of heating. At these temperatures, the elastic modulus and yield strength of the rebars were not notably reduced, as shown in Table 11a. For 90- and 120-min heated beam specimens, the ultimate loads were 222 kN and 202 kN, respectively.

4.2 Flexural Strengthening of Fire-Damaged RC Beams

The fire-exposed RC beam models were strengthened in flexure to evaluate the strengthening effect of the externally bonded steel plate and CFRP strip based on the proposed numerical model. In general, prior to strengthening application to fire-damaged RC beams, the outer layer of the beam was removed. This addressed thermally induced microcracks that could interfere with the bond between the strengthening material and the concrete. The removal of the outer concrete surface would increase construction costs and extend the duration. To avoid these, the removal of the outer damaged surface was not performed in this study. Instead, this study assumed that the plate and concrete were perfectly bonded by providing a suitable anchorage system to prevent debonding between the plate and concrete. Therefore, the strengthening material was modeled to be perfectly connected to the concrete. Externally bonded steel plate and CFRP were modeled on the bottom of the damaged beam model. The cross-sectional division dimension of the fire-damaged beam model was described and illustrated in Sect. 4.1. The material properties of the steel plate and CFRP strip used in this analytical study are summarized in Table 12. Different widths and thicknesses of strengthening materials were the variables of this investigation. 100 mm and 200 mm width were considered for both strengthening materials with a length of 3500 mm, as shown in Fig. 17. For externally bonded steel plates, thicknesses of 2 mm and 4 mm were considered as analysis variables. In the case of externally bonded CFRP strips, 0.11 mm and 0.22 mm thicknesses were used. The thickness and width of both strengthening materials were selected to provide an equal tensile force contribution to the strengthened beam models for comparison. The

Table 9 Material properties of RC beam

Concrete Beam	Tensile Reinforcement			Compressive Reinforcement			Shear Reinforcement		
f_{ck}(MPa)	*d*	f_y(MPa)	*E*(MPa)	*d*	f_y(MPa)	*E*(MPa)	*d*	f_y(MPa)	*E*(MPa)
40.3	2-D20	576	210,000	2-D8	567.2	205,000	D8	567.2	205,000
	1-D16	587	210,000						

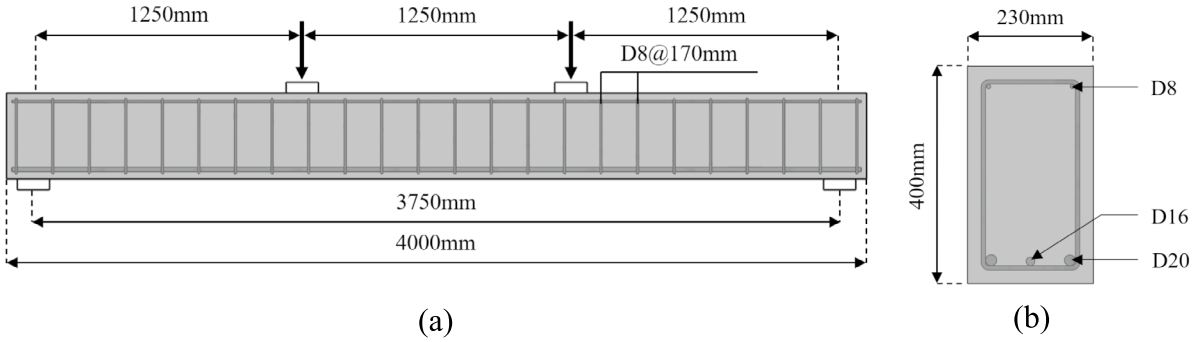

Fig. 14 Details of the beam specimens. **a** Loading arrangement. **b** Section details

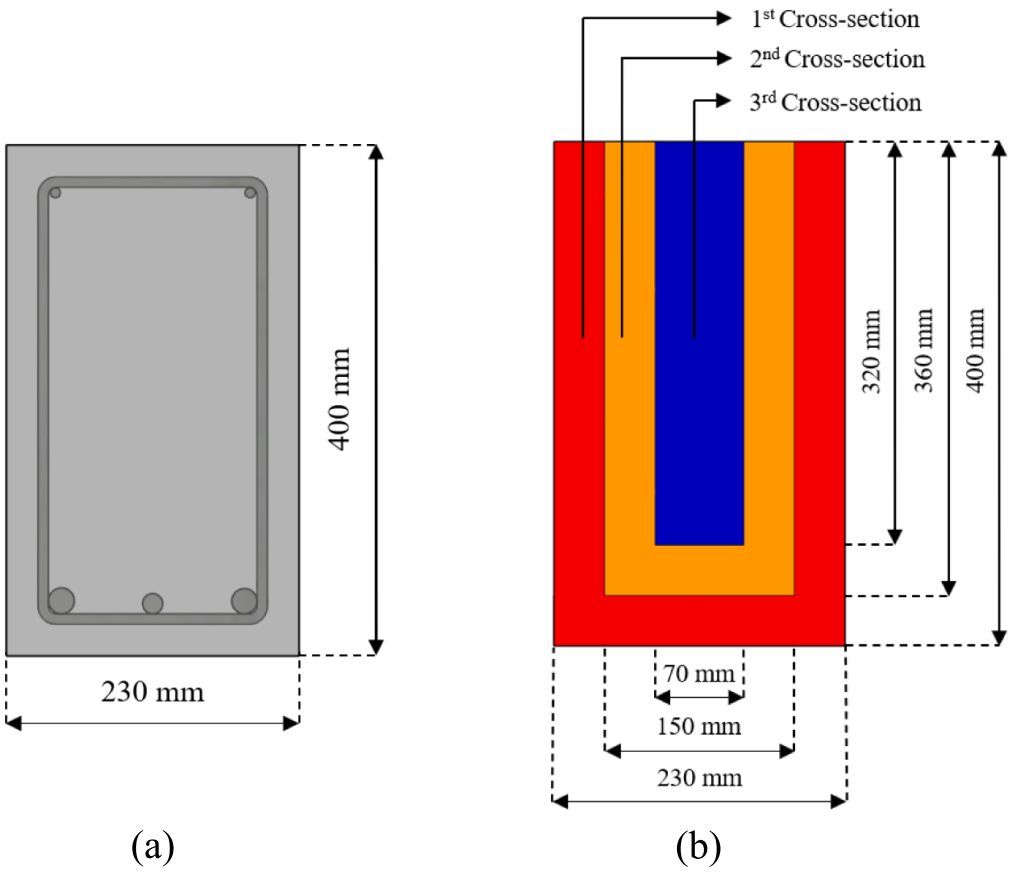

Fig. 15 Cross section of concrete beam. **a** Undamaged beam. **b** Fire-damaged beam

nomenclature of the specimens in the parametric study is shown in Fig. 18.

Fig. 19a presents the boundary conditions of the strengthened RC beam model. Only half of the beam was modeled, and strengthening materials were assumed to be perfectly bonded to concrete in both cases. Two monitoring points were used, one placed at the applied load point to measure the load increase and the other placed at midspan to measure the beam deflection. Monitoring for line conditions was applied to all tensile reinforcing bars to measure the strain of the rebars. The finite-element mesh of the strengthened beam model is shown in Fig. 19b. For the modeling of concrete, brick meshes with the size of 0.04 m were used. Both steel plate and CFRP strips were modeled using tetra meshes with a mesh size of 0.04 m.

Table 10 (a) Strength degradation of concrete cross sections (60 min heating) (b) Strength degradation of concrete cross sections (90 min heating) (c) Strength degradation of concrete cross sections (120 min heating)

Cross section	1st cross section	2nd cross section	3rd cross section
Temperature (℃)	635	243	153
Compressive strength (MPa)	16	35.4	37.2
Elastic modulus (MPa)	19,284	32,661	34,130
Temperature (℃)	725	350	233
Compressive strength (MPa)	10.6	32.3	35.6
Elastic modulus (MPa)	16,212	29,011	33,004
Temperature (℃)	788	429	319
Compressive strength (MPa)	6.8	28.5	33.5
Elastic modulus (MPa)	14,062	26,314	30,069

Table 11 (a) Strength degradation of reinforcing bars (60 min heating) (b) Strength degradation of reinforcing bars (90 min heating) (c) Strength degradation of reinforcing bars (120 min heating)

Reinforcing bar	Tensile Rebar (D20)	Tensile Rebar (D16)	Compressive Rebar	Stirrup
Temperature (℃)	525	417	411	513
Yield strength (MPa)	567.6	587	567.2	562.9
Elastic modulus (MPa)	209,318	210,000	205,000	204,654
Temperature (℃)	672	557	524	618
Yield strength (MPa)	518.3	567.5	559.3	528.3
Elastic modulus (MPa)	205,304	208,444	204,360	201,855
Temperature (℃)	777	669	612	700
Yield strength (MPa)	483.1	529.3	530.2	501.2
Elastic modulus (MPa)	202,438	205,386	202,015	199,670

5 Results and Discussion

5.1 Comparison of Load–Deflection Curves

To determine the strengthening effect, the load–deflection curves of all specimens were compared. Figure 20 presents the comparison of the load–deflection curves of all beam specimens obtained by the numerical model for 60 min heated beams. Prior to cracking, elastic behavior was shown in all of the curves. Following the first crack, the load–deflection curves of all beam models became nonlinear. After yielding of the tensile rebars, the curves increased until the peak load and then became almost stable until failure, indicating the flexural failure of the beam models. It is seen that the performance of all the strengthened beams was found to be superior in comparison with the control heated beam H-6. Before the yielding of tensile rebars, the stiffness of the CFRP-strengthened beams was similar to that of the control heated beam H-6. However, the beam specimens strengthened with CFRP exhibited a significant load increase after yielding, primarily due to the presence of CFRP on the tension side of the beam. The stiffness increase of steel plate-strengthened beams before yielding was observed to be higher than the CFRP-strengthened beams. This may be attributed to the fact that the thickness of the steel plate was significantly greater than the CFRP strip. This higher increase in stiffness of steel plate-strengthened beams resulted in a more significant decrease in deflection at ultimate load and deflection compared to beams strengthened with CFRP. The ultimate load of the CFRP-strengthened beams, namely, H-6C1-0.11, H-6C1-0.22, H-6C2-0.11, and H-6C2-0.22, increased by 7%, 12.8%, 14%, and 23.1%, respectively, as compared to the H-6 beam. For steel plate-strengthened beams, the ultimate load of beams H-6S1-2, H-6S1-4, H-6S2-2, and H-6S2-4 increased by 12%, 22.3%, 23.1%, and 43%, respectively. The ultimate original flexural capacity of the unheated beam (N-0) was effectively restored through strengthening methods using externally bonded CFRP and steel plates of the specified width and thickness. The ultimate load increase of all strengthened beams is summarized in Table 13.

The comparison of load–deflection curves of beam models for 90-min heating is shown in Fig. 21. All of the beam models exhibited very identical load–deflection response

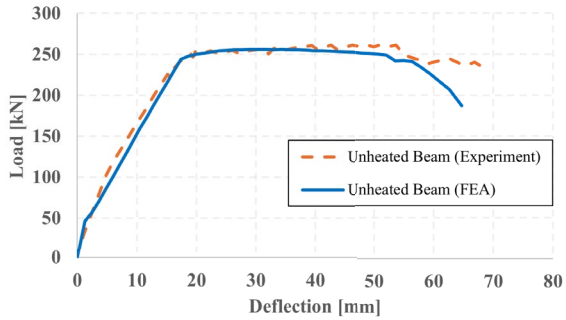

(a)

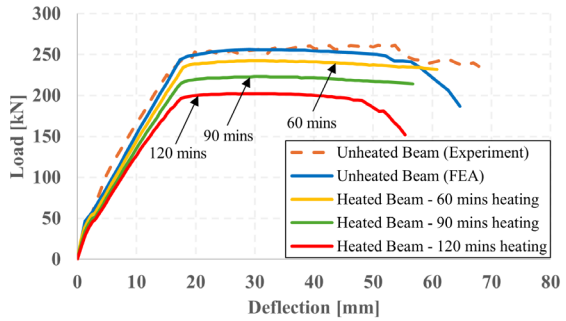

(b)

Fig. 16 Comparison of load–deflection curves between experiment and FEA. **a** Unheated beam. **b** 60 min, 90 min, and 120 min heated beam

behavior to the 60-min heated beam models. The ultimate load of the CFRP-strengthened beams H-9C1-0.11, H-9C1-0.22, H-9C2-0.11, and H-9C2-0.22 increased by 8.1%, 13.5%, 14.4%, and 24.3%, respectively, in comparison with the control heated beam H-9. The maximum load of the H-9S1-2, H-9S1-4, H-9S2-2, and H-9S2-4 beams, which were strengthened with steel plate, improved by 12.6%, 23.9%, 24.3%, and 46.4%, respectively. The initial flexural capacity of the control unheated beam (N-0) was effectively restored through both strengthening materials, except for the H-9C1-0.11 beam. The ultimate load increase of all strengthened beams is summarized in Table 14.

Fig. 22 illustrates the load–deflection curves of beam models for 120 min of heating duration. Compared with the H-12 beam, the ultimate load of the H-12C1-0.11, H-12C1-0.22, H-12C2-0.11, and H-12C2-0.22 beams increased by 6.9%, 10.9%, 11.9%, and 18.8%, respectively. The ultimate load of H-12S1-2, H-12S1-4, H-12S2-2, and H-12S2-4 increased by 12.4%, 13.4%, 22.8%, and 7.4%, respectively, for steel plate strengthened beam models. As shown in Fig. 22b, beams H-12S1-4, H-12S2-2, and H-12S2-4 failed suddenly before reaching their flexural capacity, indicating premature failures. This is attributed to the significant reduction in the compressive strength of the outer concrete after 120 min of heating. After 120 min of heating, neither of the strengthening materials was able to restore the original flexural capacity of the fire-damaged beams. The ultimate load increase of all strengthened beams is summarized in Table 15.

Table 16 summarizes the tensile force contribution of CFRP strips and steel plates, varying in width and thickness. f_t and A_t refer to the tensile (yield strength) and cross-sectional area of strengthening materials, respectively. At this particular width and thickness, both the CFRP strip and steel plate provided an equivalent tensile force of 100 kN. The comparison of load–deflection responses of strengthened beam models at 100 kN tensile force contribution by CFRP strip and steel plate is shown in Fig. 23. It is observed that all the strengthened beams had similar load–deflection response patterns at the same tensile force contributed by the strengthening material. The beam models strengthened with steel plates exhibited a higher stiffness and ultimate load capacity in comparison with the beam models strengthened with CFRP. For steel plate-strengthened beams, the tensile force of the steel plate was observed to begin distributing to the damaged beam at the initial load step. This resulted in greater improvements in stiffness before yielding and yielding load compared to the CFRP-strengthened beams. The steel plate-strengthened beams reached their ultimate load following the yielding of both the tensile rebars and the strengthening steel plate. After yielding, the load-carrying capacity of the beams began to decrease until failure. However, for CFRP-strengthened beams, the tensile force of the CFRP before yielding of tensile rebars did not significantly contribute to the damaged beam. After yielding, the CFRP started to contribute the tensile force to the beam, resulting in an increase in ultimate load.

5.2 Comparison of Tensile Rebar Strains

The maximum strain of tensile rebar in all beam models was compared to verify the efficacy of flexural strengthening performance, as shown in Fig. 24. Tensile rebar strain

Table 12 Material properties of the steel plate and CFRP strip

Steel Plate			CFRP			
E(MPa)	f_y(MPa)	t(mm)	E_f(MPa)	f_f(MPa)	ε_f	t(mm)
210,000	250	2 and 4	288,900	4,600	0.016	0.11 and 0.22

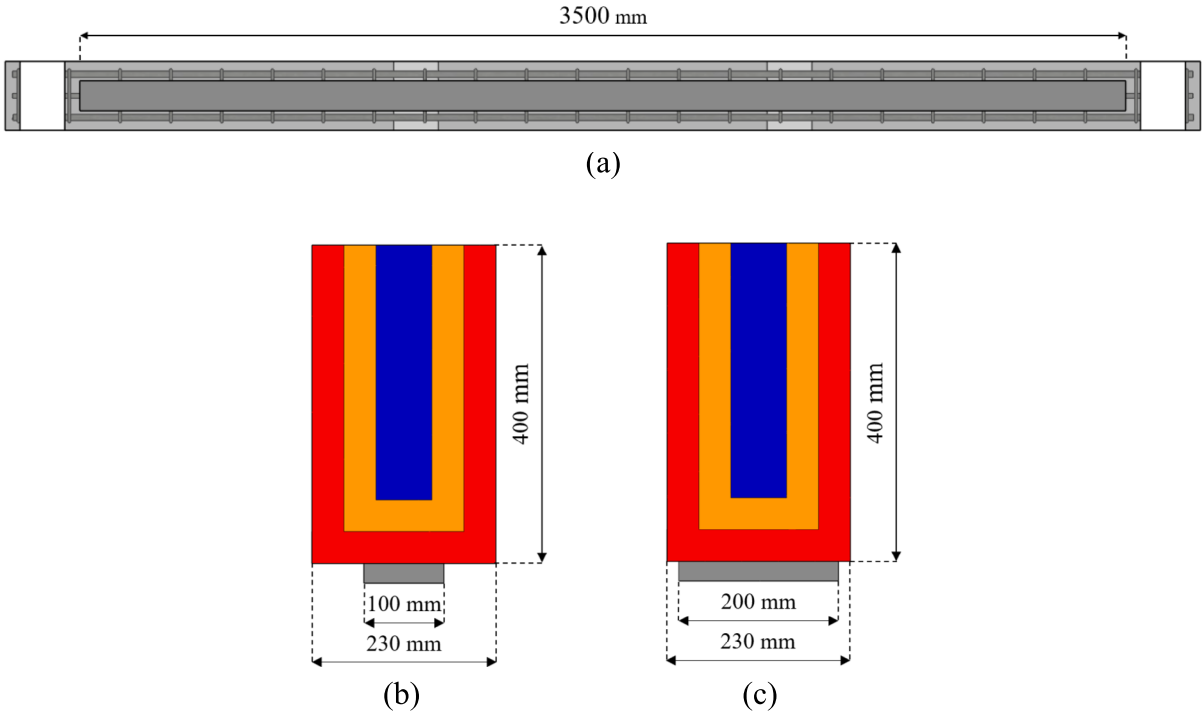

Fig. 17 Strengthening schemes of fire-damaged beam. **a** Strengthening length. **b** Strengthening width of 100 mm. **c** Strengthening width of 200 mm

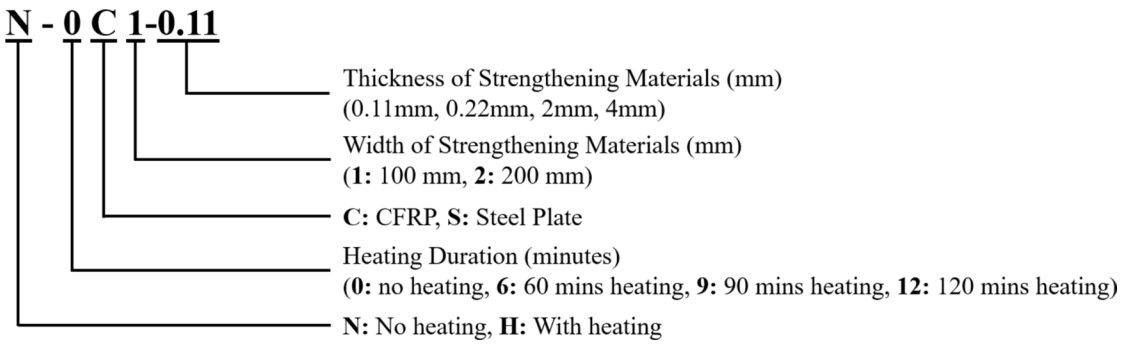

Fig. 18 Nomenclature of test specimens for parametric study

values at five different loading stages of 50 kN, 100 kN, 150 kN, yield load, and maximum load were compared. The black dashed line indicates the yield strain of the control heated beams H-6, H-9, and H-12, respectively, for each heating duration (60 min, 90 min, and 120 min). The yield strain of all three heating periods exhibited varying values as a result of changes in temperature throughout each heating duration, which led to differences in the elastic modulus and yield strength of the tensile rebar. At all loading levels, the tensile rebar strains of all strengthening beams using both methods were found to be lower than the control heated beams due to the higher stiffness of the strengthened beams.

The strain values of the tensile rebars of all strengthened beams were below the black dash line. This indicates that none of the strengthened beam models reached the yield stress at the yield load of the control heated beam. Figure 24a shows the comparison of tensile rebar strains of beam models in the case of 60 min of heating. For 60 min of heating, the yield load and ultimate load of the H-6 beam were 230 kN and 242 kN, respectively. Beams H-6C1-0.22, H-6C2-0.11, and H-6S1-4, H-6S2-2 exhibited the same strain

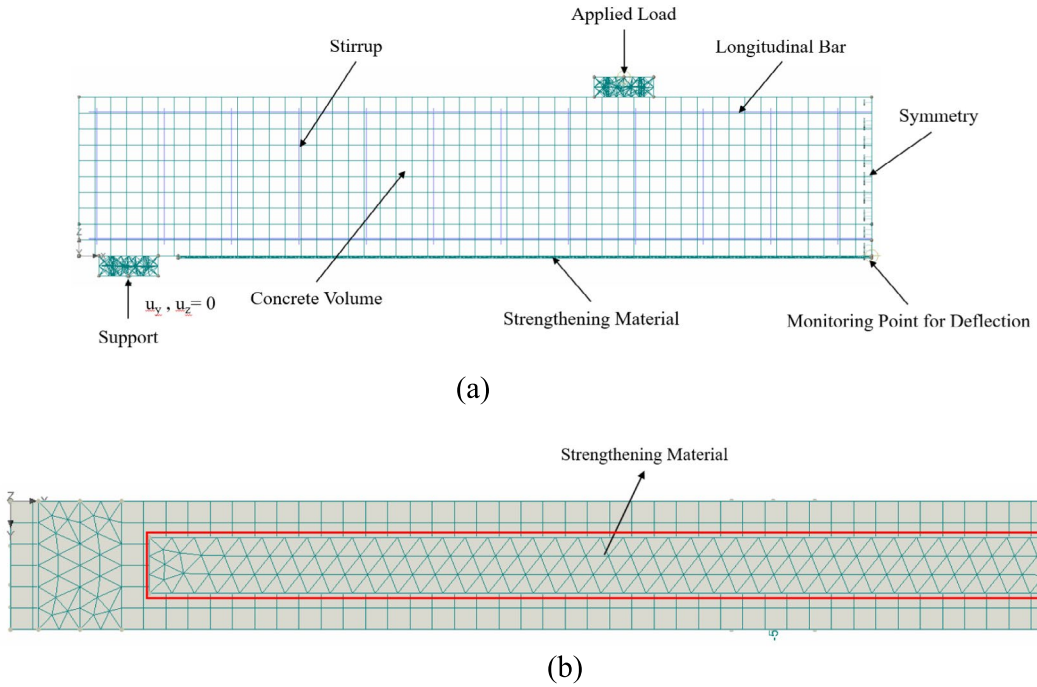

Fig. 19 Strengthened-RC beam model. **a** Boundary conditions. **b** Finite-element mesh

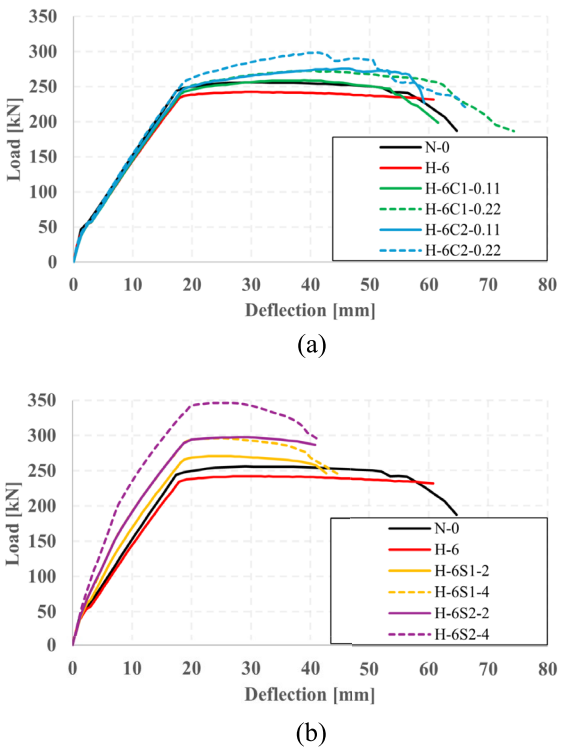

Fig. 20 Comparison of load–deflection curves of 60 min heated beam models. **a** CFRP strengthened beam models. **b** Steel plate strengthened beam models

Table 13 (a) Ultimate load increase of CFRP strengthened beams (60 min heating) (b) Ultimate load increase of steel plate strengthened beams (60 min heating)

Specimen	Ultimate Load (kN)	Increase in ultimate load (%)
H-6	242	–
H-6C1-0.11	259	7.0
H-6C1-0.22	273	12.8
H-6C2-0.11	276	14
H-6C2-0.22	298	23.1
H-6	242	–
H-6S1-2	271	12
H-6S1-4	296	22.3
H-6S2-2	298	23.1
H-6S2-4	346	43

values throughout all loading stages as a result of the same tensile force contribution from the strengthening materials. The H-6 beam showed a strain value of 0.019 at the ultimate load. At the ultimate load of 242 kN, none of the strengthened beam models yielded, except for the H-6C1-0.11 beam. For all loading stages, the CFRP strengthened beam models exhibited higher strain values than the steel plated-beam models. The comparison of tensile rebar strains in the cases of

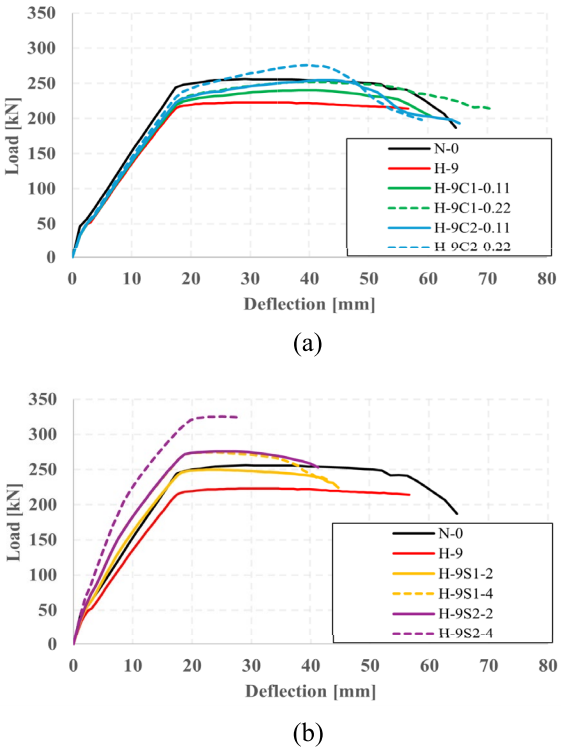

Fig. 21 Comparison of load–deflection curves of 90 min heated beam models. **a** CFRP strengthened beam models. **b** Steel plate strengthened beam models

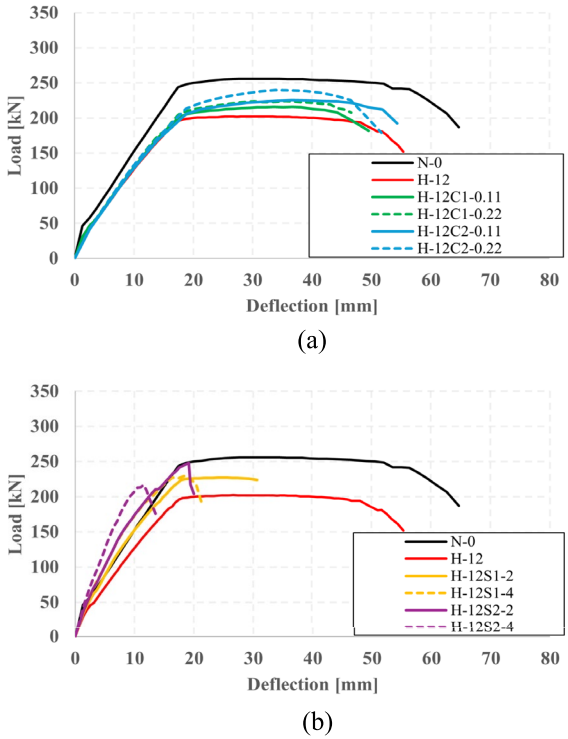

Fig. 22 Comparison of load–deflection curves of 120 min heated beam models. **a** CFRP strengthened beam models. **b** Steel plate strengthened beam models

Table 14 (a) Ultimate load increase of CFRP strengthened beams (90 min heating) (b) Ultimate load increase of steel plate strengthened beams (90 min heating)

Specimen	Ultimate Load (kN)	Increase in ultimate load (%)
H-6	222	–
H-9C1-0.11	240	8.1
H-9C1-0.22	252	13.5
H-9C2-0.11	254	14.4
H-9C2-0.22	276	24.3
H-6	222	–
H-6S1-2	250	12.6
H-6S1-4	275	23.9
H-6S2-2	276	24.3
H-6S2-4	325	46.4

Table 15 (a) Ultimate load increase of CFRP strengthened beams (120 min heating) (b) Ultimate load increase of steel plate strengthened beams (120 min)

Specimen	Ultimate load (kN)	Increase in ultimate load (%)
H-12	202	–
H-12C1-0.11	216	6.9
H-12C1-0.22	224	10.9
H-12C2-0.11	226	11.9
H-12C2-0.22	240	18.8
H-12	202	–
H-12S1-2	227	12.4
H-12S1-4	229	13.4
H-12S2-2	248	22.8
H-12S2-4	217	7.4

90-min and 120-min heating is presented in Fig. 24b, c, respectively. It can be seen that all the beam models presented similar strain distribution patterns at all loading stages to the 60-min heating beam models illustrated in Fig. 24a. The yield load and ultimate load of the H-9 beam were 210 kN and 222 kN, respectively. The H-9C1-0.11 beam showed a strain value of 0.003, which was lower compared with the H-6C1-0.11 beam. From these figures, it can be concluded that the tensile rebar strain value for all loading stages decreased

Table 16 Tensile force contribution of the steel plate and CFRP strip with different width and thickness

Materials	Width (mm)	Thickness (mm)	f_t(MPa)	$f_t.A_t$(kN)
CFRP	100	0.22	4,600	101.2
	200	0.11	4,600	101.2
Steel Plate	100	4	250	100
	200	2	250	100

as the strengthening width and thickness of the steel plate and CFRP increased.

5.3 Comparison of Concrete Strain

Figs. 25, 26, and 27 compare the strain distribution of concrete for all the beam models throughout different heating durations (60 min, 90 min, and 120 min). All the control heated H-6, H-9, and H-12 beam models showed the highest strain values that were concentrated in the middle of the beam model, representing higher flexural strains on the beams. The comparison of concrete strains for 60-min heated beam models at 230 kN is shown in Fig. 25. The strain values of the control heated H-6 beam in the figure were the highest, around 0.0031, in comparison with the other beam models. For all the strengthened beam models, the strain contour color started to change, revealing the deduction of concrete strain compared to the control heated beam H-6. Among all the strengthened beam models, the H-6S2-4 beam exhibited the lowest strain value (0.0014). The next lowest strain distribution value was 0.0023 for H-6S2-2. These results indicate that increasing the thickness and width of the strengthening materials can reduce the concrete strain resulting from flexural loading. The comparison of concrete strains of beam models for 90 min of heating at 210 kN is presented in Fig. 26. The strain distribution patterns of the control heated beam and the strengthened beam models in the case of 90-min heating were found to be highly comparable with the 60-min heated beam models, as shown in Fig. 25.

Fig. 27 shows the distribution of concrete strain in 120-min heated beam models at a load of 192 kN. It can be observed that all of the strengthened beams demonstrated lower concrete strain distribution in the middle region compared to H-12. As the width and thickness of both strengthening materials increased, a decrease in the concrete strain distribution was observed. In the figure, H-12S1-4, H-12S2-2, and H-12S2-4 exhibited notable strain at the end plate of the strengthening steel plate, which exhibited a different strain distribution pattern compared to shorter heating durations (60 min and 90 min). The occurrence of a high strain distribution value on that region was due to the stress resulting from the very strong adhesive bond strength of the steel plate bonded to the beam, as well as the significant strength degradation of the first concrete cross section after 120 min of heating. This stress continued until failure resulted in brittle failure prior to the yielding of the reinforcing bars and the strengthening steel plate. These are shown in the load–deflection curves of the H-12S1-4, H-12S2-2, and H-12S2-4 beams, as presented in Fig. 22b.

6 Conclusion

This paper presented an analytical study on the flexural strengthening of fire-damaged RC beams. The proposed simplified methodology was validated with previous experimental research for evaluating the residual flexural capacity after fire exposure. The reference beams were then subjected to the ISO standard fire curve for 60 min, 90 min, and 120 min, respectively. Furthermore, the damaged beam models were strengthened in flexure with different widths and thicknesses using the externally bonded reinforcement (EBR) techniques for evaluating the flexural response of the fire-damaged beams. The main conclusions obtained from this study are summarized as below:

1. The strength degradation model of concrete and reinforcing bars after a fire has a great influence on evaluating the residual flexural capacity of fire-damaged members. Different strength degradation models can be considered to optimize the accuracy of the numerical model.
2. This simplified cross-sectional approach based on finite-element analysis can be applicable for analyzing the post-fire flexural response of beams. Various heating curves and durations can be applied to this model for evaluating the capacity of the RC beam after being exposed to fire for strengthening consideration.
3. The flexural strengthening performance of fire-damaged RC beams can be investigated by utilizing a variety of strengthening schemes and materials from the built-in material model of the finite-element analysis software.
4. This model can be a useful tool for the design of the strengthening material strength required to fulfill the original design criteria of the fire-damaged RC beams, depending on heating duration and conditions.
5. All the strengthened fire-damaged beam models exhibited higher flexural capacity and stiffness compared to the fire-damaged beams without strengthening for all heating durations. As the width and thickness of the strengthening materials increase, there is a greater improvement in the stiffness, yield load,

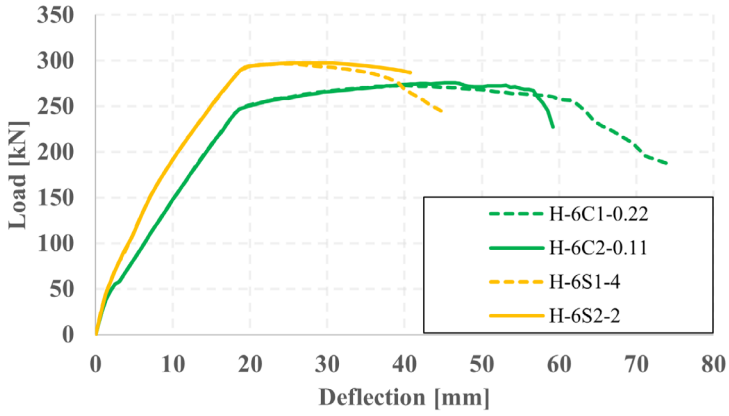

(a)

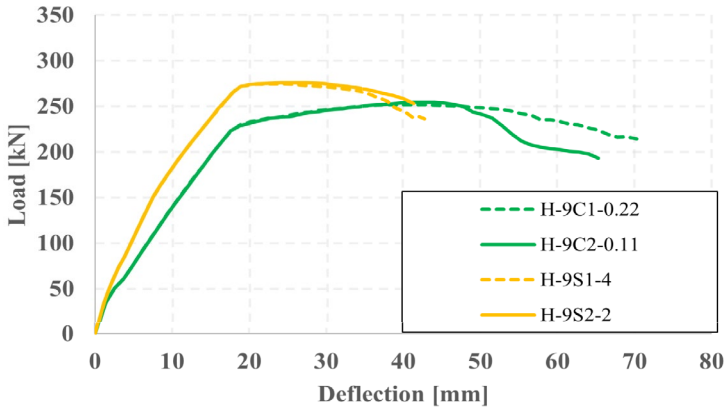

(b)

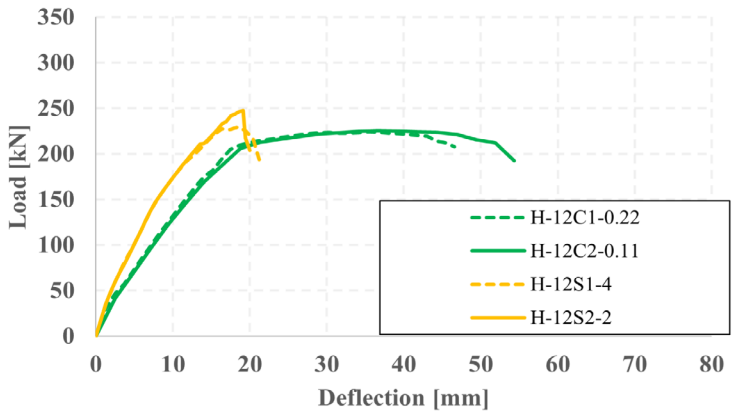

(c)

Fig. 23 Comparison of load–deflection curves of strengthened beam models at the tensile force contribution of 100 kN. **a** 60 min heated strengthened beam models. **b** 90 min heated strengthened beam models. **c** 120 min heated strengthened beam models

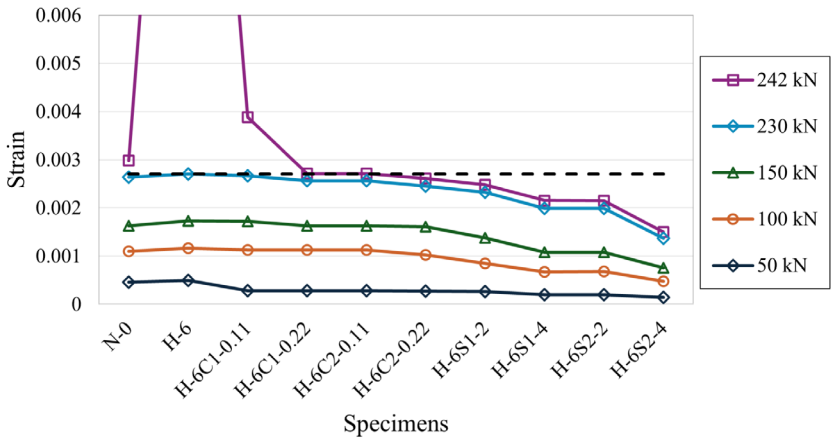

(a)

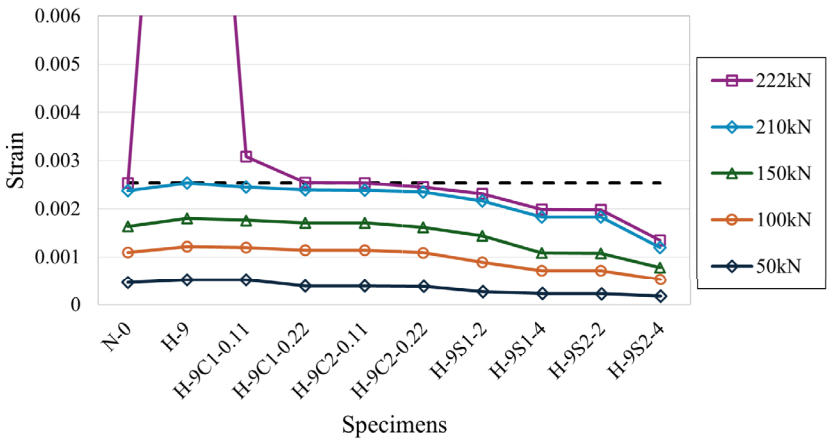

(b)

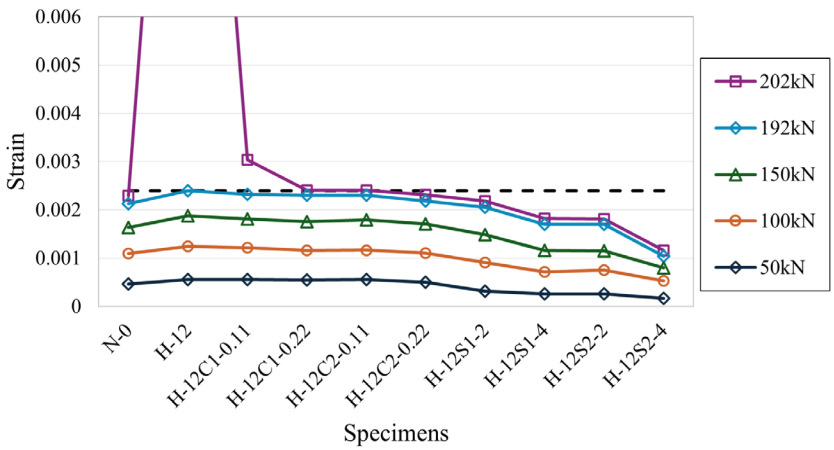

(c)

Fig. 24 Comparison of tensile rebar strain. **a** 60 min heated beam models. **b** 90 min heated beam models. **c** 120 min heated beam models

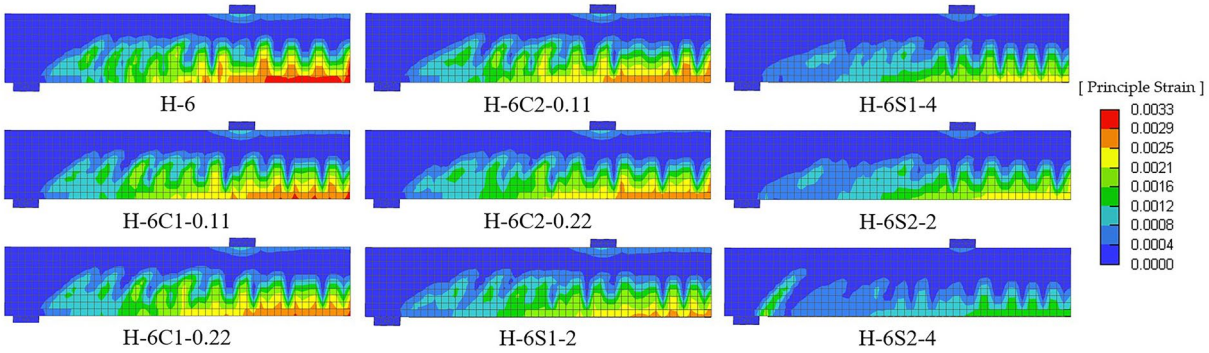

Fig. 25 Comparison of concrete strains of 60 min heated beam models

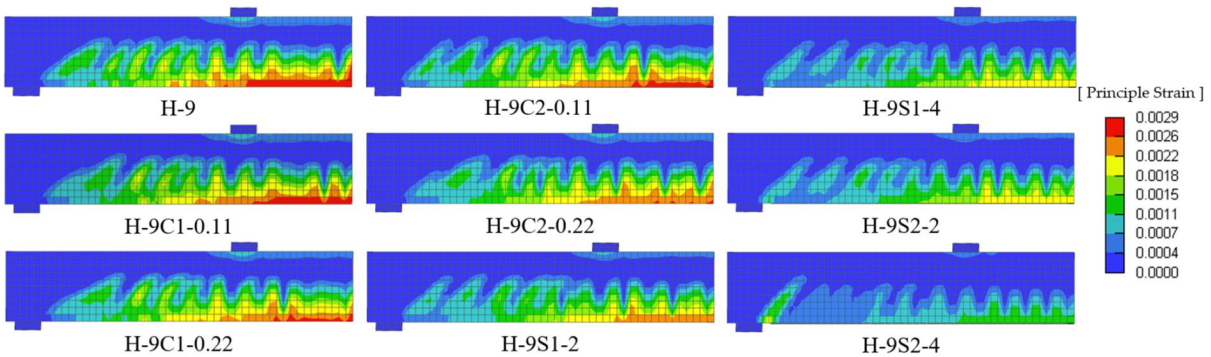

Fig. 26 Comparison of concrete strains of 90 min heated beam models

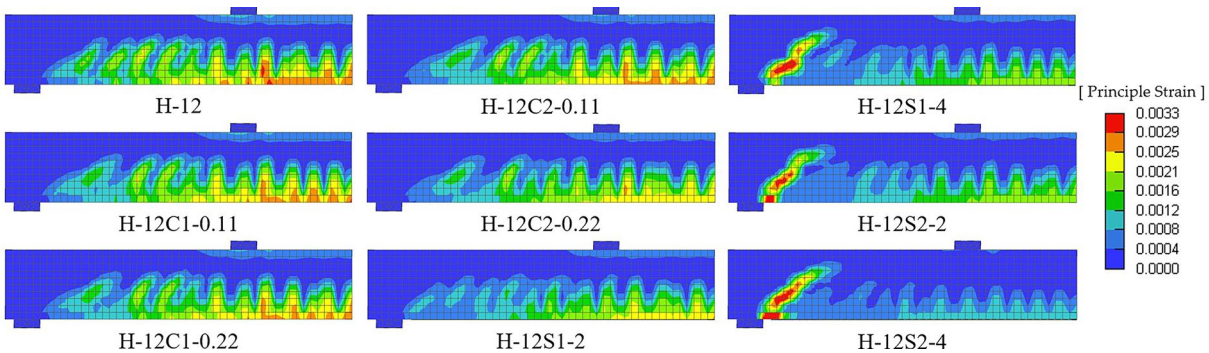

Fig. 27 Comparison of concrete strains of 120 min heated beam models

and ultimate load of the damaged beams. However, after 120 min of heating, the steel plate-strengthened beams exhibited brittle failure, primarily attributed to the substantial reduction in the compressive strength of the outer concrete.

6. Both strengthening techniques investigated in this study can be considered to be promising methods for recovering the flexural capacity of fire-damaged beams. Externally bonded steel plates demonstrated a greater enhancement in stiffness and ultimate load capacity compared to externally bonded CFRP strips.
7. The outer part of the fire-damaged beam (1st concrete cross section) experienced severe damage as the heating duration increased. After 120 min of heating, the first concrete cross section should be replaced with newly cast concrete to improve bond behavior between the strengthening materials and the concrete, thereby enhancing the flexural strengthening performance of the beams.

Although this simplified cross-sectional method reasonably described the flexural behavior of fire-damaged beams, certain simplifications made in this study require further improvement to accurately describe the residual flexural capacity of RC beams and the performance of flexural strengthening. These include the residual ultimate strength of reinforcing bars after fire, the bond-slip behavior of concrete and rebars before and after fire exposure, the removal of the outer concrete cross section before strengthening application, the modeling of the interface between concrete and plate, and the validation of the experimental study on fire-damaged beams with the application of strengthening materials, which will be considered in the future study.

Acknowledgements
This work was supported by INHA UNIVERSITY Research Grant.

Author contributions
Lybundith Eng: investigation, data curation, formal analysis, validation, and writing—original draft. Changhyuk Kim: conceptualization, methodology, funding acquisition, resource, supervision, and review and editing.

Availability of data and materials
Data will be made available upon request.

Declarations

Ethics approval and consent to participate
All authors of the manuscript confirm the ethics approval and consent to participate following the Journal's policies.

Consent for publication
All authors of the manuscript agree on the publication of this work in the International Journal of Concrete Structures and Materials.

Competing interests
The authors declare that they have no known competing financial interests or personal relationships that could have appeared to influence the work reported in this paper.

Received: 21 August 2024 Accepted: 28 March 2025
Published online: 04 May 2025

References

Abdallah, M., Al Mahmoud, F., Boissiere, R., Khelil, A., & Mercier, J. (2020). Experimental study on strengthening of RC beams with side near surface mounted technique-CFRP bars. *Composite Structures, 234*, 111716. https://doi.org/10.1016/j.compstruct.2019.111716

Ahmad, M. S., & Bhargava, P. (2023). Effect of different load levels on the flexure performance of RC beams exposed to fire. *Materials Today Proceedings*. https://doi.org/10.1016/j.matpr.2023.04.684

Alam, M. A., Onik, S. A., & Mustapha, K. N. B. (2020). Crack based bond strength model of externally bonded steel plate and CFRP laminate to predict debonding failure of shear strengthened RC beams. *Journal of Building Engineering, 27*, 100943. https://doi.org/10.1016/j.jobe.2019.100943

Aldhafairi, F., Hassan, A., Abd-EL-Hafez, L., & Abouelezz, A. (2020). Different techniques of steel jacketing for retrofitting of different types of concrete beams after elevated temperature exposure. *Structures*. https://doi.org/10.1016/j.istruc.2020.09.017

Altin, S., Anil, Ö., & Kara, M. E. (2005). Improving shear capacity of existing RC beams using external bonding of steel plates. *Engineering Structures, 27*(5), 781–791. https://doi.org/10.1016/j.engstruct.2004.12.012

Anasco Bastin, D. R., Sharma, U. K., & Bhargava, P. (2017). A study on different techniques of restoration of fire damaged reinforced concrete flexural members. *Journal of Structural Fire Engineering, 8*(2), 131–148. https://doi.org/10.1108/JSFE-03-2017-0026

Baluch, M. Flexural behaviour of precracked reinforced concrete beams strengthened externally by steel plates. *Flexural Behaviour Of Precracked Reinforced Concrete Beams Strengthened Externally By Steel Plates,* **92**(1), 14–23.

Barnes, R. A., & Mays, G. C. (2006). Strengthening of reinforced concrete beams in shear by the use of externally bonded steel plates: Part 1 Experimental programme. *Construction and Building Materials*, *20*(6), 396–402. https://doi.org/10.1016/j.conbuildmat.2005.01.034.

Belakhdar, A. R., Dimia, M. S., Baghdadi, M., Bouderradji, M., Gherabli, S., & Alaoui, N. (2023). Post-fire behavior and repair of fire-damaged RC columns using composite jackets. *Annales De Chimie Science des Matériaux*. https://doi.org/10.18280/acsm.470407

Büyüköztürk, O., Taşdemir, M. A., Felicetti, R., & Gambarova, P. (2013). Assessment of the residual strength of fire-damaged steel-rebars. *Nondestructive Testing of Materials and Structures*. https://doi.org/10.1007/978-94-007-0723-8_31

Cervenka, J., Surovec, J., & Kabele, P. (2020). Modelling of reinforced concrete structures subjected to fire. In *Computational Modelling of Concrete Structures* (pp. 515–522). CRC Press.

Červenka, V., Jendele, L., & Červenka, J. (2021). ATENA Program Documentation–Part 1. *Cervenka Consulting sro*.

Ciampa, E., Ceroni, F., De Angelis, A., & Pecce, M. R. (2023). Bond tests on concrete elements externally bonded with steel plates and assessment of bond strength models. *Engineering Structures, 296*, 116835. https://doi.org/10.1016/j.engstruct.2023.116835

da Costa, L. M., de Carvalho Pires, T. A., & Silva, J. J. R. (2023). Shear strengthening of fire-damaged reinforced concrete beams using NSM CFRP laminates. *Engineering Structures, 287*, 116175. https://doi.org/10.1016/j.engstruct.2023.116175

European Committee for Standardization. (2004). *EN 1992-1-2: Eurocode 2: Design of concrete structures – Part 1-2: General rules – Structural fire design*.

Fayyadh, M. M., & Razak, H. A. (2021). Externally bonded FRP applications in RC structures: A state-of-the-art review. *Jordan Journal of Civil Engineering*, 15(2), 157–179 (2021)

Hamoda, A. A., Eltaly, B. A., Sera, R. E., & Liang, Q. Q. (2023). Behavior of reinforced concrete stair slabs strengthened with steel plates and near surface mounted steel bars. *Engineering Structures, 292*, 116514. https://doi.org/10.1016/j.engstruct.2023.116514

Hamoush, S. A., & Ahmad, S. (1990). Debonding of steel plate-strengthened concrete beams. *Journal of Structural Engineering, 116*(2), 356–371. https://doi.org/10.1061/(ASCE)0733-9445(1990)116:2(356)

Hao, M., Zheng, W., & Chang, W. (2022). Evaluation of axial load-bearing capacity of concrete columns strengthened by a new section enlargement method. *Journal of Civil Engineering and Management, 28*(1), 25–38. https://doi.org/10.3846/jcem.2021.15855

Haroon, M., Moon, J. S., & Kim, C. (2021). Performance of reinforced concrete beams strengthened with carbon fiber reinforced polymer strips. *Materials, 14*(19), 5866. https://doi.org/10.3390/ma14195866

Huang, Z. (2010). The behaviour of reinforced concrete slabs in fire. *Fire Safety Journal, 45*(5), 271–282. https://doi.org/10.1016/j.firesaf.2010.05.001

Hussain, Q., Ruangrassamee, A., Joyklad, P., & Wijeyewickrema, A. C. (2022). Shear enhancement of rc beams using low-cost natural fiber rope reinforced polymer composites. *Buildings, 12*(5), 602. https://doi.org/10.3390/buildings12050602

Jadooe, A., Al-Mahaidi, R., & Abdouka, K. (2017). Experimental and numerical study of strengthening of heat-damaged RC beams using NSM CFRP strips. *Construction and Building Materials, 154*, 899–913. https://doi.org/10.1016/j.conbuildmat.2017.07.202

Jadooe, A., Al-Mahaidi, R., & Abdouka, K. (2018a). Behaviour of heat-damaged partially-insulated RC beams using NSM systems. *Construction and Building Materials, 180*, 211–228. https://doi.org/10.1016/j.conbuildmat.2018.05.279

Jadooe, A., Al-Mahaidi, R., & Abdouka, K. (2018b). Performance of heat-damaged partially-insulated RC beams strengthened with NSM CFRP strips

and epoxy adhesive. *Construction and Building Materials, 159*, 617–634. https://doi.org/10.1016/j.conbuildmat.2017.11.020
Jendele, L., Šmilauer, V., & Červenka, J. (2014). Multiscale hydro-thermo-mechanical model for early-age and mature concrete structures. *Advances in Engineering Software, 72*, 134–146. https://doi.org/10.1016/j.advengsoft.2013.05.002
Jiang, C.-J., Lu, Z.-D., & Li, L.-Z. (2017). Shear performance of fire-damaged reinforced concrete beams repaired by a bolted side-plating technique. *Journal of Structural Engineering, 143*(5), 04017007. https://doi.org/10.1061/(ASCE)ST.1943-541X.0001726
Joyklad, P., Sirisonthi, A., Chaiyasarn, K., Hussain, Q., & Suparp, S. (2023). Structural behavior of full-scale precast posttensioned girder with substandard transverse reinforcement–experimental and analytical study. *Structural Concrete, 24*(1), 634–652. https://doi.org/10.1002/suco.202100787
Kar, S., & Biswal, K. (2021). External shear strengthening of RC beams with basalt fiber sheets: an experimental study. *Structures*. https://doi.org/10.1016/j.istruc.2021.01.094
Kim, C., Jirsa, J. O., & Ghannoum, W. M. (2017). Performance of concrete panels reinforced with carbon fiber-reinforced polymer materials. *Journal of Composites for Construction, 21*(3), 04016100. https://doi.org/10.1061/(ASCE)CC.1943-5614.0000758
Kodur, V., & Agrawal, A. (2016). An approach for evaluating residual capacity of reinforced concrete beams exposed to fire. *Engineering Structures, 110*, 293–306. https://doi.org/10.1016/j.engstruct.2015.11.047
Li, L.-Z., Jiang, C.-J., Yu, J.-T., Wang, X., & Lu, Z.-D. (2019). Flexural performance of fire-damaged reinforced concrete beams repaired by bolted side-plating. *ACI Structural Journal*. https://doi.org/10.14359/51713319
Li, X., Lu, X., Qi, J., & Bao, Y. (2022). Flexural behavior of fire-damaged concrete beams repaired with strain-hardening cementitious composite. *Engineering Structures, 261*, 114305.
Lou, T., Lopes, A., & Lopes, S. (2012). Influence of span-depth ratio on behavior of externally prestressed concrete beams. *ACI Structural Journal*. https://doi.org/10.14359/51684046
Lou, T., Lopes, S. M., & Lopes, A. V. (2013). Flexural response of continuous concrete beams prestressed with external tendons. *Journal of Bridge Engineering, 18*(6), 525–537.
Ma, W., Yin, C., Zhou, J., & Wang, L. (2019). Repair of fire-damaged reinforced concrete flexural members: a review. *Sustainability, 11*(19), 5199. https://doi.org/10.3390/su11195199
Mejía, N., Sarango, A., & Espinosa, A. (2024). Flexural and shear strengthening of RC beams reinforced with externally bonded CFRP laminates postfire exposure by experimental and analytical investigations. *Engineering Structures, 308*, 117995. https://doi.org/10.1016/j.engstruct.2024.117995
Moon, J. S., Kim, D. Y., Ko, M. S., & Kim, C. (2023). Performance of reinforced concrete beams strengthened by bidirectional carbon-fiber-reinforced polymers based on numerical models. *Polymers, 15*(4), 1012. https://doi.org/10.3390/polym15041012
Oller, E., Pujol, M., & Marí, A. (2019). Contribution of externally bonded FRP shear reinforcement to the shear strength of RC beams. *Composites Part B: Engineering*, *164*, 235–248. https://doi.org/10.1016/j.compositesb.2018.11.065.
Sabar, A. H. A., & Kadhum, M. M. (2022). Numerical modeling of the experimental test for shear strengthened of fire damaged high strength lightweight RC beams with SIFCON jacket. *Periodicals of Engineering and Natural Sciences, 10*(2), 512–538.
Sadaghian, H., Mirrezaei, S. S., & Farzam, M. (2023). Numerical simulation of punching shear in RC slabs subjected to elevated temperatures. *Magazine of Concrete Research, 76*(1), 1–19. https://doi.org/10.1680/jmacr.22.00350
Shang, X.-Y., Yu, J.-T., Li, L.-Z., & Lu, Z.-D. (2020). Shear strengthening of fire damaged RC beams with stirrup reinforced engineered cementitious composites. *Engineering Structures, 210*, 110263. https://doi.org/10.1016/j.engstruct.2020.110263
Shareef, N. A., & Kadhum, M. M. (2025). Numerical simulation of post fire-behaviour of high strength lightweight reinforced concrete beams strengthened with basalt fiber-reinforced polymer grid and engineered cementitious composites jacket. *Journal of Building Pathology and Rehabilitation, 10*(1), 14. https://doi.org/10.1007/s41024-024-00523-2
Su, R., Lam, W., & Pam, H. (2008). Behaviour of embedded steel plate in composite coupling beams. *Journal of Constructional Steel Research, 64*(10), 1112–1128. https://doi.org/10.1016/j.jcsr.2007.09.013
Sundarraja, M., & Rajamohan, S. (2009). Strengthening of RC beams in shear using GFRP inclined strips–an experimental study. *Construction and Building Materials, 23*(2), 856–864. https://doi.org/10.1016/j.conbuildmat.2008.04.008
Tao, Z., Wang, X.-Q., & Uy, B. (2013). Stress-strain curves of structural and reinforcing steels after exposure to elevated temperatures. *Journal of Materials in Civil Engineering, 25*(9), 1306–1316. https://doi.org/10.1061/(ASCE)MT.1943-5533.0000676
Thanaraj, D. P., Anand, N., Arulraj, P., & Al-Jabri, K. (2020). Investigation on structural and thermal performance of reinforced concrete beams exposed to standard fire. *Journal of Building Engineering, 32*, 101764. https://doi.org/10.1016/j.jobe.2020.101764
Thamrin, R., & Sari, R. P. (2017). Flexural capacity of strengthened reinforced concrete beams with web bonded steel plates. *Procedia Engineering*, *171*, 1129–1136. https://doi.org/10.1016/j.proeng.2017.01.474.
Tianlai, Y., Shuai, T., Yunpeng, Z., & Liyuan, Z. (2016). Experimental and theoretical investigation of bending in concrete beams strengthened with external prestressing CFRP tendons. *The Open Construction & Building Technology Journal*. https://doi.org/10.2174/1874836801610010492
Van Cao, V., Vo, H. B., Dinh, L. H., & Van Doan, D. (2022). Experimental behavior of fire-exposed reinforced concrete slabs without and with FRP retrofitting. *Journal of Building Engineering, 51*, 104315. https://doi.org/10.1016/j.jobe.2022.104315
Vilnay, O. (1988). The analysis of reinforced concrete beams strengthened by epoxy bonded steel plates. *International Journal of Cement Composites and Lightweight Concrete, 10*(2), 73–78. https://doi.org/10.1016/0262-5075(88)90033-4
Wang, Y. D., Yang, S., Han, M., & Yang, X. (2013). Experimental study of section enlargement with reinforced concrete to increase shear capacity for damaged reinforced concrete beams. *Applied Mechanics and Materials, 256*, 1148–1153. https://doi.org/10.4028/www.scientific.net/AMM.256-259.1148
Yang, K.-H. (2019). Axial behavior of reinforced concrete columns strengthened with new section enlargement approaches. *ACI Structural Journal*. https://doi.org/10.14359/51715631
Zhang, J., Teng, J., Wong, Y., & Lu, Z. (2001). Behavior of two-way RC slabs externally bonded with steel plate. *Journal of Structural Engineering, 127*(4), 390–397. https://doi.org/10.1061/(ASCE)0733

Publisher's Note

Lybundith Eng is a master's student in the Department of Architectural Engineering at Inha University, Republic of Korea.

Changhyuk Kim Changhyuk Kim is an Assistant Professor in the Department of Architectural Engineering at Inha University. He received his PhD from the University of Texas at Austin, Austin, TX. His research interests include the repair and retrofit of reinforced concrete structures using carbon fiber reinforced polymers.